

**Angular, spectral, and time distributions of highest energy protons and associated secondary gamma rays and neutrinos propagating through extragalactic magnetic and radiation fields**F. A. Aharonian,<sup>1,3,\*</sup> S. R. Kelner,<sup>2,3,†</sup> and A. Yu. Prosekin<sup>3,‡</sup><sup>1</sup>*Dublin Institute for Advanced Studies, 31 Fitzwilliam Place, Dublin 2, Ireland*<sup>2</sup>*Moscow Institute of Engineering Physics, Kashirskoe shosse 31, Moscow, 115409 Russia*<sup>3</sup>*Max-Planck-Institut für Kernphysik, Saupfercheckweg 1, D-6917 Heidelberg, Germany*

(Received 8 June 2010; published 5 August 2010)

The angular, spectral, and temporal features of the highest energy protons and, accompanying them, secondary neutrinos and synchrotron gamma rays propagating through the intergalactic magnetic and radiation fields are studied using the analytical solutions of the Boltzmann transport equation obtained in the limit of the small-angle and continuous-energy-loss approximation.

DOI: [10.1103/PhysRevD.82.043002](https://doi.org/10.1103/PhysRevD.82.043002)

PACS numbers: 96.50.sb, 13.85.Tp, 98.70.Rz, 98.70.Sa

**I. INTRODUCTION**

Because of deflections in the interstellar and intergalactic magnetic fields (IGMF), the information about the original directions of cosmic rays pointing to their production sites is lost. On the other hand, the isotropic flux of cosmic rays is contributed, most likely, by a large number of galactic and extragalactic sources. These objects represent different source populations characterized by essentially different physical parameters—age, distance, energy budget, etc., as well as by different particle acceleration scenarios. This makes extremely difficult the identification of sources of cosmic rays based on the chemical composition and energy spectra of particles—two measurables characterizing the “soup” (isotropic flux of cosmic rays) cooked over cosmological time scales. Fortunately, at extremely high energies,  $E \sim 10^{20}$  eV, the impact of galactic and extragalactic magnetic fields on the propagation of cosmic rays becomes less dramatic, which might result in large and small scale anisotropies of cosmic ray fluxes. Thus, depending on the strength and structure of the (highly unknown) IGMF, the highest energy domain of cosmic rays may offer us a new astronomical discipline—“cosmic ray astronomy.” The extension of studies to energies  $10^{20}$  eV and beyond enhances the chances of localization of particle accelerators for two reasons. With an increase of particle energy, the probability that a proton would penetrate through the intergalactic medium (IGM) without significant deflections in chaotic magnetic fields increases. Note that for IGMF much weaker than  $10^{-9}$  G, the deflection angle can be quite small also for lower energy protons ( $\theta \propto B/E$ ). However, at energies significantly below  $10^{20}$  eV, the deflection in galactic magnetic fields becomes the dominant factor leading to the lost of information about the original directions of particles (see, e.g., Ref. [1]).

In the context of prospects of realization of “cosmic ray astronomy,” there is a second *independent* factor which gives strong preference to energies  $10^{20}$  eV. Particles of such high energies can arrive only from relatively nearby accelerators located within 100 Mpc (see, e.g., [2]). This dramatically (by orders of magnitude) decreases the number of relevant sources of  $\geq 10^{20}$  eV protons contributing to the observed cosmic ray flux, and correspondingly reduces the level of the diffuse background, i.e. the (quasi) isotropic flux as a superposition of contributions by unresolved discrete sources. Formally, one cannot *a priori* exclude the possibility that the  $10^{20}$  eV cosmic rays are contributed by a large number of weak sources which cannot be detected individually. Alternatively, the entire cosmic ray flux at such high energies can be dominated by contributions from a few sources, especially given the tough requirements to the  $10^{20}$  eV proton accelerators [3]. This excludes, in particular, objects like ordinary galaxies, unless the galaxies provide highest energy cosmic rays through transient events related to compact objects like gamma ray bursts (GRB) [4].

The propagation of cosmic rays in IGMF has been discussed in a number of recent works (see, e.g., Refs. [5–8]). In these studies different magnetized environments have been assumed and different methods dealing with particle transport have been applied. Consequently, their conclusions are quite different, the principal reason being the different assumptions and approaches in the modeling of the IGMF. The main purpose of our work is to study the features related to the transport of particles, therefore we assume, following Ref. [7], purely turbulent and homogeneous IGMF. We limit our treatment by only the proton component of cosmic rays, and associated with it the secondary gamma rays and neutrinos. This not only makes the calculations simple and more transparent (as long as it concerns the pure transport effects), but also seems to be a feasible realization for the large scale structure of IGMF.

Whether we may identify the accelerators of extragalactic cosmic rays using the highest energy protons is a question which largely depends on the strength of the large

\*Felix.Aharonian@mpi-hd.mpg.de

†Stanislav.Kelner@mpi-hd.mpg.de

‡Anton.Prosekin@mpi-hd.mpg.de

scale IGMF. Even for the most favorable conditions for realization of the “proton astronomy,” the latter will be relevant to the nearby Universe, the accessible sources being limited within a sphere of radius 100 Mpc. A different approach for localization of acceleration cites of  $10^{20}$  eV protons can be provided by observations of gamma rays and neutrinos produced at interactions of these energetic particles with the 2.7 K CMBR photons and magnetic fields in the proximity of the source, namely, within a region of a size of order of 10 Mpc—sufficiently large for effective interaction of protons with 2.7 K photons through the photomeson process and, at the same time, still small for a significant deflection of protons from their original directions. All short-lived particles of these interactions, as well as the products of their decays (gamma rays, neutrinos, and electrons) are produced at small angles relative to the initial directions of parent protons. In an magnetized environment with  $B \geq 10^{-9}$  G the electrons with typical energy exceeding  $10^{19}$  eV are predominantly cooled via synchrotron radiation with production of high energy gamma rays. The electrons emit synchrotron photons very quickly, before any significant change of their direction in the surrounding chaotic magnetic field. Thus the synchrotron photons will move essentially in the initial direction of the parent protons. Since the protons, after they escape their production site (accelerator), move radially, the observer will see an apparent compact (quasi-pointlike) gamma-ray source [9,10], even though gamma rays are produced in an extended region with angular size of order of  $\sim d/r \sim 5(r/100 \text{ Mpc})^{-1}$  deg. Note that the same is true if protons escape the source anisotropically, but are moving within a narrow angular cone towards the observer. Otherwise, the observer will miss the source.

The favorable range of IGMF for realization of this scenario is  $10^{-9}$ – $10^{-7}$  G. In a stronger magnetic field, deflections of protons are significant even at the first several Mpc scales. Thus, because of the small interaction depth of undeviated protons, the pointlike source becomes very weak.

On the other hand, for IGMF much weaker than  $10^{-9}$  G electrons are cooled predominantly via inverse Compton scattering, thus the efficiency of synchrotron radiation drops dramatically. This scenario, which involves a pair cascade in the 2.7 CMBR and extragalactic background radiation (EBL), also leads to high energy gamma rays. However, unless the field is much weaker than  $10^{-12}$  G, the cascade electrons of relatively low (TeV) energies are thermalized, thus the cascade leads to the formation of giant halos [11] and in this way contributes to the diffuse extragalactic gamma-ray background radiation (see, e.g., Ref. [12]) rather than to the formation of a discrete gamma-ray source (for a discussion of different regimes of formation of cascades initiated by interactions of highest energy protons with 2.7 K CMBR, and their detectability from the direction of the cosmic ray source see Ref. [13]).

The detection of the cascade component as a pointlike or a slightly extended source of gamma rays initiated by interactions of ultrahigh energy protons (after they escape the accelerator) with 2.7 K CMBR is possible in the case of extremely small IGMF,  $B \leq 10^{-15}$  G (see, e.g., Ref. [14]).

The energy spectrum and flux of synchrotron radiation of secondary electrons from photomeson interactions of protons with 2.7 K CMBR have been studied in Ref. [10]. The calculations have been limited by the first 10 Mpc range of propagation of protons, assuming that at this stage protons propagate radially without significant deviations, and the secondary electrons move along the same direction before they emit synchrotron photons. While this approximation gives a correct estimate of the flux, it does not specify the angle within which the radiation is confined. This approach ignores also the non-negligible tails of distribution of synchrotron radiation formed at the later stages of propagation and interactions of protons.

In the case of quasicontinuous operation of an extragalactic accelerator of protons over time scales exceeding the typical delay time due to the deflection in the magnetic field, the energy and angular distributions of protons, as well as accompanying photons and electrons, can be accurately described by the steady-state solutions of the transport equations. Generally, this is the case of a continuous proton accelerator of age  $T \geq 10^6$  yr. In the case of shorter activity of the source (an “impulsive accelerator”) or solitary events like GRB, relatively simple analytical solutions of the arrival time distributions of protons, gamma rays, and neutrinos can be obtained within an approximation when the energy losses of protons are ignored. We consider the cases of “continuous” and “impulsive” proton accelerations in Secs. II and IV, respectively.

## II. STEADY STATE DISTRIBUTION FUNCTIONS

The realization of the small-angle multiple scattering considerably simplifies the description of propagation of protons through a scattering medium. In particular, in the small-angle approximation the term  $\mathbf{v} \frac{\partial f}{\partial r}$  of the Boltzmann transport equation can be presented in a form allowing analytical derivation of the steady state solution. Because of the smallness of the single scattering angle, one can write the elastic collision integral in the Fokker-Planck approximation. To expand the distribution function into series in terms of the single scattering angle one should have a smooth function of this angle. This condition is satisfied if one neglects the unscattered part of the distribution function that has very sharp angle dependency. Such an approximation is justified in the case of multiple scattering.

The approach provides solutions that can be applied to the various cases which, independent of the details of the scattering medium, are characterized only by the average scattering angle per unit length  $\langle \theta_s^2 \rangle$ . The scattering process depends on the particle energy, i.e.  $\langle \theta_s^2 \rangle$  is a function of

energy. During the propagation through the medium between two scattering centers, the energy of particles is gradually decreased due to different dissipative processes. If the change of energy in each action of interaction is considerably smaller than the initial energy, one can use the continuous energy approximation. It should be noted that in the approach described here, the processes responsible for the scattering and the energy loss of particles are not required to be the same. The particle scattering could have elastic character and do not cause energy losses. On the other hand, the effect of deflection of particles from their original direction due to the processes responsible for energy losses might be negligibly small. This is the case of the problem considered below. One can safely ignore the change of the direction of primary particles as well as the production angles ( $\theta \sim 1/\gamma$ ) of the secondary products (gamma rays, electrons, neutrinos) due to all relevant processes including photomeson and pair production, inverse Compton scattering, synchrotron radiation.

The aim of this section is to derive distribution functions for protons and accompanying them secondary particles propagating through the galactic and extragalactic magnetic fields for a spherically symmetric point source of protons. However, it is technically more convenient to consider first a source emitting protons in a given (fixed) direction. In this case we have a preferential direction along the infinitely narrow beam emitted by the source. Let us choose the  $z$ -axis along this direction. Because of the scattering, particles deviate from the initial course. To define the deviation we introduce angles  $\theta_x$  and  $\theta_y$  between the direction of propagation  $\mathbf{n}$  and the coordinate planes YOZ and XOZ, respectively. If  $\mathbf{n}$  is close to the  $z$ -axis, the angles  $\theta_x$  and  $\theta_y$  are small and can be treated as components of two-dimensional vector  $\boldsymbol{\theta}$  in the XOY plane, where the absolute value of  $\boldsymbol{\theta}$  corresponds to the deflection angle between  $\mathbf{n}$  and the  $z$ -axis. Then we can write  $\mathbf{n} \approx (\theta_x, \theta_y, 1 - \frac{\theta^2}{2}) = (\boldsymbol{\theta}, 1 - \frac{\theta^2}{2})$ .

The retention of the second-order term  $\theta^2/2$  in the expansion of  $n_z$  allows us to take into account the effects relating to the elongation of the path like delay time, but does not give any considerable contribution to steady-state solution. Therefore, we divide the problem into two sub-problems. In the first part of the paper, we solve the steady-state equation that takes into account the energy losses but ignores the elongation of particle trajectories. The results of these calculations are relevant to the continuous source of protons and describe the energy and angular distributions of protons and accompanying neutrinos and synchrotron radiation of secondary electrons produced during the propagation of protons. In the second part of the paper, we calculate the distributions of arrival times of protons, neutrinos and gamma rays in the case of an impulsive source. In this case the arrival time delays directly depend on the elongation of trajectory. The time-dependent solutions for distribution functions presented in Sec. IV are limited by

the approximation in which the energy losses of protons are neglected.

Thus, to derive the steady-state solution of the transport equation we assume  $\mathbf{n} \approx (\theta_x, \theta_y, 1) = (\boldsymbol{\theta}, 1)$ . Let us denote by  $\boldsymbol{\rho} = (x, y)$  the perpendicular displacement in the plane XOY. For a point source characterized by a monoenergetic and infinitely narrow beam of protons emitted along the  $z$ -axis we obtain the equation for Green function  $G(\mathbf{r}, \boldsymbol{\theta}, E)$  of the Boltzmann steady-state transport equation in the approximations of a small-angle multiple scattering and continuous energy losses:

$$\left(\frac{\partial}{\partial z} + \boldsymbol{\theta} \frac{\partial}{\partial \boldsymbol{\rho}} - \frac{\langle \theta_s^2 \rangle}{4} \frac{\partial^2}{\partial \theta^2} - \frac{\partial}{\partial E} \bar{\epsilon}\right) G(\mathbf{r}, \boldsymbol{\theta}, E, E_0) = \frac{1}{c} \delta(z) \delta(\boldsymbol{\rho}) \delta(\boldsymbol{\theta}) \delta(E - E_0). \quad (1)$$

Here we take into account that the particles are ultrarelativistic  $|\mathbf{v}| = c$ . The solution of Eq. (1) is obtained in Ref. [15] for the propagation of charged particles passing through a layer of matter. The features of this solution are comprehensively discussed in Ref. [16]. Using the notations introduced in Ref. [16], the Green function can be written in the form:

$$G(\mathbf{r}, \boldsymbol{\theta}, E, E_0) = \frac{\delta(S(E, E_0) - z)}{c \bar{\epsilon}(E) \pi^2 \Delta} \times \exp\left(-\frac{A_1 \boldsymbol{\rho}^2 - 2A_2 \boldsymbol{\theta} \boldsymbol{\rho} + A_3 \theta^2}{\Delta}\right), \quad (2)$$

where  $S$  is the traveled distance that is uniquely related to the energy loss rate  $\bar{\epsilon}(E) = |dE/dz|$ :

$$S(E, E_0) = \int_E^{E_0} \frac{dE'}{\bar{\epsilon}(E')}, \quad (3)$$

and

$$\Delta = A_1 A_3 - A_2^2. \quad (4)$$

The  $\delta$ -function in Eq. (2) points to the fact that we neglect the elongation of trajectory so the traveled distance is equal to  $z$  as if particles propagate strictly along  $z$ -axis. Taking the relation between energy and  $z$  into account,  $A_i$  can be written in the following form:

$$A_i(E_0, z) = \int_0^z \langle \theta_s^2 \rangle(z')(z - z')^{i-1} dz'. \quad (5)$$

It is easy to recognize the physical meanings of the coefficients  $A_1$ ,  $A_2$ , and  $A_3$ ;  $A_1$  is the mean square deflection angle,  $A_3$  is the mean square displacement, and  $A_2$  is the mean value of  $\boldsymbol{\theta} \boldsymbol{\rho}$  at the distance  $z$ :

$$A_1 = \langle \theta^2 \rangle_z, \quad A_2 = \langle \boldsymbol{\theta} \boldsymbol{\rho} \rangle_z, \quad A_3 = \langle \boldsymbol{\rho}^2 \rangle_z. \quad (6)$$

For the treatment of the case of spherically symmetric point source of protons, let us rewrite the Green function in the form which is independent of choice of the coordinate system. After the replacements

$$\boldsymbol{\theta} \rightarrow \mathbf{n} - \mathbf{n}_0, \quad \boldsymbol{\rho} \rightarrow \mathbf{r} - r\mathbf{n}_0, \quad z \rightarrow r, \quad (7)$$

where  $\mathbf{n}_0$  is the direction of the emission,  $\mathbf{n}$  is the direction of particle motion at the point  $\mathbf{r}$ , we find

$$G(\mathbf{r}, \mathbf{n}, \mathbf{n}_0, E, E_0) = \frac{\delta(S(E, E_0) - r)}{c\bar{\epsilon}(E)\pi^2\Delta} \exp\left(-\frac{A_1(\mathbf{r} - r\mathbf{n}_0)^2 - 2A_2(\mathbf{r} - r\mathbf{n}_0)(\mathbf{n} - \mathbf{n}_0) + A_3(\mathbf{n} - \mathbf{n}_0)^2}{\Delta}\right). \quad (8)$$

Performing integration over all directions of the vector  $\mathbf{n}_0$  by the saddle point method (see Appendix A), we find

$$G_{\text{sph}}(r, \theta, E, E_0) = \frac{\delta(S(E, E_0) - r)}{c\bar{\epsilon}(E)r^2\pi D} \exp\left(-\frac{\theta^2}{D}\right), \quad (9)$$

where

$$D = A_1 - 2\frac{A_2}{r} + \frac{A_3}{r^2}. \quad (10)$$

Since we have spherically symmetric distribution, the Green function depends only on the distance  $r$  from the source and  $\theta$  which is the angle between the radius-vector from the source to the observation point and the movement direction at this point.

We assume that the spherically symmetric source injects protons into the IGM with a constant rate:

$$Q_p(\mathbf{r}, E) = cJ_p(E)\delta(\mathbf{r}). \quad (11)$$

The substitution of this expression into

$$f(r, \theta, E) = \int Q(\mathbf{r}_0, E_0)G_{\text{sph}}(r - r_0, \theta, E, E_0)d\mathbf{r}_0dE_0 \quad (12)$$

gives

$$f_p(r, \theta, E) = \frac{1}{\bar{\epsilon}(E)} \int_E^\infty \frac{J_p(E_0)}{\pi r^2 D} \exp\left(-\frac{\theta^2}{D}\right) \delta(S(E, E_0) - r) dE_0, \quad (13)$$

where  $D$  can be written as

$$D(E_0, r) = \frac{1}{r^2} \int_0^r \langle \theta_s^2 \rangle (r') r'^2 dr'. \quad (14)$$

For the given energy and spatial distribution of protons we can calculate the number of secondary particles from the decays of  $\pi$ -mesons that are produced at interactions between protons and 2.7 K CMBR photons. To obtain the energy distributions of the secondary products—photons, electrons, and neutrinos, we use the approximation proposed in Ref. [17]. The energy of protons is ultrarelativistic so we can assume that secondary particles initially move in the same direction as protons. The distribution of second particles can be presented in the form

$$Q(r, \theta, E) = \hat{Q}(f_p(r, \theta, E_p)) \quad (15)$$

where  $\hat{Q}$  denotes an integral operator. For example, for the energy distribution of protons  $J_p(E)$ , the energy distribution of photons produced in photomeson interactions is

$$Q_\gamma(E_\gamma) = \hat{Q}_\gamma(J_p(E_p)), \quad (16)$$

where

$$\hat{Q}_\gamma(J_p(E_p)) = \int J_p(E_p) f_{\text{ph}}(\epsilon) w(E_\gamma, E_p, \epsilon) dE_p d\epsilon. \quad (17)$$

Here  $f_{\text{ph}}$  is the distribution function of CMBR photons,  $w$  is the differential interaction rate of the  $p\gamma$  interactions, namely, the Bethe-Heitler pair production or photomeson production (see Ref. [17]). Since we are interested in the distribution of ultrarelativistic electrons that weakly deviate in the magnetic field, we can apply the Green function given by Eq. (8) to the source function given by Eq. (15). Note that  $\hat{Q}$  acts only on variable  $E_p$ , therefore we can change the order of integration. Tedious calculations (see Appendix B) yield:

$$f_e(r, \theta, E_e) = \frac{1}{c\bar{\epsilon}_e(E_e)} \int_{E_e}^\infty dE_{e0} \hat{Q}_e \left[ \frac{1}{\bar{\epsilon}_p(E_p)} \int_{E_p}^\infty dE_{p0} \times \frac{J_p(E_{p0}) \exp\left(-\frac{\theta^2}{D_e + D_p}\right)}{r^2 \pi(D_e + D_p)} \delta(S - r) \right]. \quad (18)$$

Here  $S$  is sum of the distances traveled by proton to the point of interaction with CMRB and traveled by electron from the point of production to the point  $r$ :

$$S = S_p(E_p, E_{p0}) + S_e(E_e, E_{e0}). \quad (19)$$

The angular distribution of electrons in Eq. (18) is characterized by

$$D_e = A_{e1} - 2\frac{A_{e2}}{r} + \frac{A_{e3}}{r^2}, \quad (20)$$

where  $A_{ei} = A_{ei}(E_e, E_{e0})$  have the same meaning as in Eq. (5), and

$$D_p = \frac{1}{r^2} \int_0^{r_0} \langle \theta_s^2 \rangle r'^2 dr', \quad (21)$$

where  $r_0 = S_p(E_p, E_{p0})$ .

The main channel of production of gamma rays by HE electrons is synchrotron radiation. Applying the modified Eq. (D1) for the spectrum of synchrotron radiation in chaotic magnetic field to the distribution of electrons given by Eq. (18), we find the angular and spatial distributions of gamma ray. Let us describe the procedure as in Eq. (15) by

$$Q_s(r, \theta, E_\gamma) = \hat{Q}_s(f_e(r, \theta, E_e)). \quad (22)$$

In the general case the distribution function of gamma rays

that are characterized by the source function  $Q(\mathbf{r}, \mathbf{n}, E)$  and propagate through the absorbing medium with extinction coefficient  $k(E)$ , is

$$f_\gamma(\mathbf{r}, \mathbf{n}, E) = \frac{1}{c} \int_0^\infty Q(\mathbf{r} - \mathbf{n}\tau, \mathbf{n}, E) e^{-k\tau} d\tau, \quad (23)$$

where  $\mathbf{n}$  is the direction of movement at the point  $\mathbf{r}$  that coincides with the direction of emitting as the propagation of gamma rays is rectilinear. Since emitting electrons have ultrarelativistic energy, we assume that the direction of radiation coincide with the electron direction, therefore the distribution function of synchrotron gamma rays for the distribution of electrons given by Eq. (18) is

$$f_\gamma(r, \theta, E_\gamma) = \frac{1}{c} \int_0^\infty \hat{Q}_s(f_e(|\mathbf{r} - \mathbf{n}\tau|, \theta_i, E_e)) e^{-k(E_\gamma)\tau} d\tau, \quad (24)$$

where  $\theta_i$  is the angle between  $\mathbf{n}$  and  $\mathbf{r} - \mathbf{n}\tau$ , and  $\theta$  is the angle between  $\mathbf{n}$  and  $\mathbf{r}$ . It is convenient to perform the integration over  $\tau$  using the delta function in Eq. (18). For that we should change the order of integration so the integration over  $\tau$  becomes internal. Using the features of the delta function we find

$$\frac{\delta(|\mathbf{r} - \mathbf{n}\tau| - S)}{|\mathbf{r} - \mathbf{n}\tau|^2} = \frac{1}{Sr} \frac{1}{\sqrt{(\frac{S}{r})^2 - \sin^2\theta}} \sum_{i=1}^2 \delta(\tau - \tau_i), \quad (25)$$

where  $\tau_{1,2} = r(\cos\theta \mp \sqrt{(\frac{S}{r})^2 - \sin^2\theta})$ . Since the term corresponding to  $\tau_2$  does not contribute to large angles  $\theta_i$  in exponent [see Eq. (18)] we keep only the term corresponding to  $\tau_1$ . After performing relevant calculations we obtain:

$$f_\gamma(\mathbf{r}, \theta, E_\gamma) = \hat{Q}_s \left\{ \frac{1}{c^2 \bar{\epsilon}_e(E_e)} \int_{E_e}^\infty dE_{e0} \hat{Q}_e \left[ \frac{1}{\bar{\epsilon}_p(E_p)} \times \int_{E_p}^\infty dE_{p0} \tilde{f}_p \eta \left( 1 - \frac{S}{r} \right) \eta \left( \frac{S}{r} - \sin\theta \right) \right] \right\}, \quad (26)$$

where

$$\tilde{f}_p = \frac{J_p(E_{p0})}{\frac{S}{r} \sqrt{(\frac{S}{r})^2 - \sin^2\theta}} \frac{\exp(-\frac{\theta_1^2}{D_e + D'_p})}{\pi r^2 (D_e + D'_p)} e^{-k(E_\gamma)\tau_1}, \quad (27)$$

$\eta$  is the Heaviside function. The angle between  $\mathbf{n}$  and  $\mathbf{r} - \mathbf{n}\tau$  is

$$\theta_1 = \arccos \left( \frac{\sqrt{(S/r)^2 - \sin^2\theta}}{S/r} \right). \quad (28)$$

### III. THE SPECTRAL AND ANGULAR DISTRIBUTIONS OF PROTONS, PHOTONS, AND NEUTRINOS

#### A. Protons

Transport of protons substantially depends on the spatial distribution of magnetic fields. The assumption of chaotically oriented magnetic cells is usually used for estimates of the influence of IGMF on cosmic-ray propagation (see, e.g., Ref. [18]). The spectral analysis of the correlation function of the magnetic field fluctuations [19] provides a more appropriate and accurate treatment of the problem. We use this approach for derivation of the mean square deflection angle.

UHE protons propagate large distances in IGMF without considerable deflections. Indeed, the evaluation of the deflection angle  $\delta\theta \simeq \lambda/r_g$  on the correlation length  $\lambda$  is

$$\delta\theta \simeq 9 \times 10^{-3} \left( \frac{\lambda}{1 \text{ Mpc}} \right) \left( \frac{B}{10^{-9} \text{ G}} \right) \left( \frac{10^{20} \text{ eV}}{E} \right) \text{ rad}, \quad (29)$$

where  $r_g = E/eB$  is the gyroradius of the ultrarelativistic particle. Therefore, change of direction of ultrahigh energy protons is small on the scale  $\lambda \simeq 1 \text{ Mpc}$ . The proton energy can be assumed constant for this scale. Then the proton motion in the magnetic field is described by the equation

$$\dot{\mathbf{v}} = \frac{ec}{E} [\mathbf{v} \times \mathbf{B}(\mathbf{r})]. \quad (30)$$

For ultrarelativistic particles  $\mathbf{v} = c\mathbf{n}$ , where  $\mathbf{n}$  is a unit vector. Rewriting the change in velocity over the time  $\Delta t$  in the form  $\Delta\mathbf{v} = c\boldsymbol{\theta}$ , we find

$$\boldsymbol{\theta} = \int_t^{t+\Delta t} \frac{ec}{E} [\mathbf{n} \times \mathbf{B}(\mathbf{r}(t))] dt. \quad (31)$$

Since the deflection angle is small, the trajectory of particle can be considered rectilinear in integration.

Now one should make an assumption about the statistical properties of the magnetic fields. Here we assume that IGMF is a statistically isotropic and homogeneous. While  $\langle\boldsymbol{\theta}\rangle = 0$  (since in this case  $\langle\mathbf{B}\rangle = 0$ ), the mean square deflection is

$$\begin{aligned} \langle\boldsymbol{\theta}^2\rangle &= \left( \frac{ec}{E} \right)^2 \int \langle [\mathbf{n} \times \mathbf{B}_1][\mathbf{n} \times \mathbf{B}_2] \rangle dt_1 dt_2 \\ &= \left( \frac{e}{E} \right)^2 (\delta_{\alpha\beta} - n_\alpha n_\beta) \int \langle B_{1\alpha} B_{2\beta} \rangle dz_1 dz_2, \end{aligned} \quad (32)$$

where  $\mathbf{B}_{1,2} = \mathbf{B}(\mathbf{r}(t_{1,2}))$ . Here we switch to integration over coordinates of particle, directing the  $z$ -axis along  $\mathbf{n}$ .

Equation (32) includes the correlation function of the magnetic field

$$K_{\alpha\beta}(\mathbf{r}_1 - \mathbf{r}_2) \equiv \langle B_\alpha(\mathbf{r}_1) B_\beta(\mathbf{r}_2) \rangle. \quad (33)$$

It depends only on the difference  $(\mathbf{r}_1 - \mathbf{r}_2)$  because we assume statistical homogeneity of the magnetic field. The

mean square of magnetic field is determined as  $\langle \mathbf{B}^2 \rangle = K_{\alpha\alpha}(0) = \text{const}$ .

To turn to the spectral description,  $K_{\alpha\beta}$  should be written as a Fourier integral:

$$K_{\alpha\beta}(\mathbf{r}_1 - \mathbf{r}_2) = \int \tilde{K}_{\alpha\beta}(\mathbf{k}) e^{i\mathbf{k}(\mathbf{r}_1 - \mathbf{r}_2)} \frac{d^3k}{(2\pi)^3}. \quad (34)$$

Since  $\text{div} \mathbf{B} = 0$ , then  $K_{\alpha\beta}$  should satisfy the conditions

$$\partial K_{\alpha\beta} / \partial x_{1\alpha} = 0, \quad \partial K_{\alpha\beta} / \partial x_{2\beta} = 0. \quad (35)$$

For function  $\tilde{K}_{\alpha\beta}$  these conditions take on form  $\tilde{K}_{\alpha\beta} k_\alpha = 0$ ,  $\tilde{K}_{\alpha\beta} k_\beta = 0$ . Therefore, if there is no preferential direction in space,  $\tilde{K}_{\alpha\beta}$  has the following structure:

$$\tilde{K}_{\alpha\beta}(\mathbf{k}) = \frac{1}{2} \left( \delta_{\alpha\beta} - \frac{k_\alpha k_\beta}{k^2} \right) \Phi(k^2) \langle \mathbf{B}^2 \rangle. \quad (36)$$

Here constant factor  $\langle \mathbf{B}^2 \rangle$  is introduced such that  $\Phi(k^2)$  meets the normalization condition:

$$\int \Phi(k^2) \frac{d^3k}{(2\pi)^3} = \frac{1}{2\pi^2} \int_0^\infty \Phi(k^2) k^2 dk = 1. \quad (37)$$

It is convenient to change variables  $z_1 = z + \zeta/2$ ,  $z_2 = z - \zeta/2$  in the integral in Eq. (32). Assuming that the traveled distance  $\Delta z$  is much greater than a characteristic scale on which the correlation function tends to zero, one can extend the limits of integration over  $\zeta$  to infinity. Meanwhile, the traveled distance should be smaller than the distance on which the proton loses its energy appreciably. The integrand depends only on  $\zeta$ , therefore the integration over  $d\zeta$  gives the length of integration interval  $\Delta z$ . The mean square deflection angle is proportional to the traveled distance, so the mean square deflection per unit length is

$$\langle \theta_s^2 \rangle = \left( \frac{e}{E} \right)^2 (\delta_{\alpha\beta} - n_\alpha n_\beta) \int_{-\infty}^\infty K_{\alpha\beta}(0, 0, \zeta) d\zeta. \quad (38)$$

Integration of  $K_{\alpha\beta}$  written in the form of Eq. (34) over  $d\zeta$  gives  $2\pi\delta(k_z)$  that allows us to calculate the integral over  $dk_z$ . Then, the integral remains over the components of  $\mathbf{k}$  perpendicular to  $z$ -axis. Using Eq. (36), we obtain

$$\langle \theta_s^2 \rangle = \frac{1}{2} \left( \frac{e}{E} \right)^2 \langle \mathbf{B}^2 \rangle \int \frac{d^2k_\perp}{(2\pi)^2} \Phi(k_\perp^2). \quad (39)$$

The derived result can be written in the form

$$\langle \theta_s^2 \rangle = \frac{\pi}{2} \left( \frac{e}{E} \right)^2 \langle \mathbf{B}^2 \rangle \Lambda, \quad (40)$$

where

$$\Lambda = \int \frac{d^3k}{(2\pi)^3} \frac{1}{k} \Phi(k^2) = \frac{1}{2\pi^2} \int_0^\infty \Phi(k^2) k dk. \quad (41)$$

Taking into account Eq. (37), the factor  $\Lambda$  can be treated as the mean value of  $k^{-1}$ ,  $\Lambda = \langle k^{-1} \rangle$ .

The calculation of  $\langle \theta_s^2 \rangle$  requires the spectral energy distribution of magnetic field. To obtain final form of  $\langle \theta_s^2 \rangle$  we assume a power-law spectrum

$$\Phi(k^2) k^2 \sim \begin{cases} \left( \frac{k_0}{k} \right)^\alpha, & k > k_0 \\ \left( \frac{k}{k_0} \right)^\beta, & k < k_0 \end{cases} \quad (42)$$

where  $k_0$  is an absolute value of the wave vector corresponding to the maximal scale of correlation  $\lambda$ :  $k_0 = 2\pi/\lambda$ . It gives

$$\langle \theta_s^2 \rangle = \frac{(\alpha - 1)(\beta + 1)}{4\alpha\beta} \left( \frac{e}{E} \right)^2 \langle \mathbf{B}^2 \rangle \lambda. \quad (43)$$

Taking into account the turbulent character of IGMF that has  $\langle \mathbf{B} \rangle = 0$ , we take  $\alpha = 5/3$  which corresponds to the Kolmogorov turbulence. The choice of the parameter  $\beta$  is, to a certain extent, arbitrary. Here we assume  $\beta = 1$  which leads to a simple expression for the mean square deflection angle per unit length:

$$\langle \theta_s^2 \rangle = \frac{\lambda}{5} \left( \frac{e}{E} \right)^2 \langle \mathbf{B}^2 \rangle. \quad (44)$$

Because of uncertainties related to the spectrum of IGMF, the numerical factor in Eq. (44) is somewhat different from the coefficients used in other papers (see, e.g., Ref. [18]).

Significant uncertainty in calculations of  $\langle \theta_s^2 \rangle$  is related to the absolute value of the correlation length  $\lambda$ . It is expected to be between 100 kpc and 1 Mpc, i.e. comparable to the characteristic distances between galaxies. In the subsequent calculations we normalize the correlation length to  $\lambda = 1$  Mpc, but the presented results can be easily recalculated for any  $\lambda$ .

Since the propagation of protons in IGMF can be treated as a set of large number of small chaotic deflections, the problem can be reduced to the diffusion in angle. The diffusion coefficient  $D(r, E_0)$  given by Eq. (14) contains information about the energy loss and influence of IGMF on propagation, and gives angular distribution of protons at the given point. Since there is a unique correspondence between the energy and  $r$  [see Eq. (9)] we can rewrite Eq. (14) in terms of energy and energy losses per unit length. Substituting Eq. (44) into Eq. (14), we obtain

$$D(E, E_0) = \frac{\eta}{r^2} \int_E^{E_0} \frac{1}{E'^2} \left( \int_{E'}^{E_0} \frac{dE''}{\bar{\epsilon}(E'')} \right)^2 \frac{dE'}{\bar{\epsilon}(E')}, \quad (45)$$

where

$$r = \int_E^{E_0} \frac{dE'}{\bar{\epsilon}(E')}, \quad \eta = \frac{e^2 \lambda}{5} \langle \mathbf{B}^2 \rangle. \quad (46)$$

The function  $E/\bar{\epsilon}(E)$  based on results of Ref. [17] and implying the mean free path of protons in the IGM due to the Bethe-Heitler pair production and photomeson processes at interactions with CMBR, is shown in Fig. 1. The results of these calculations are in a good agreement with

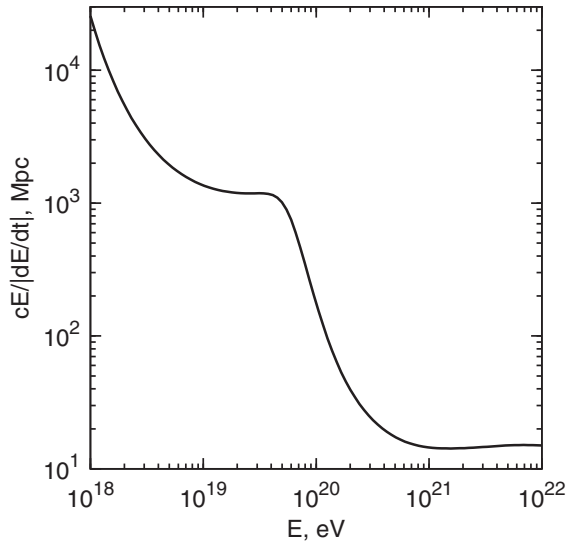


FIG. 1. The mean free path of protons in the IGM due to interactions with photons of CMBR.

[20], except for the region above  $10^{21}$  eV where the discrepancy is approximately 20%. The reason for the difference is presumably due to the slightly different cross sections used in Refs. [20,21].<sup>1</sup> Note that for many scenarios described by Eq. (1) the same process is responsible for both the angular scattering and the energy losses. But in the case of propagation of protons in the IGM we deal with two different processes: while the interactions with CMBR lead to energy losses, the angular deflections are caused by multiple scattering on magnetic inhomogeneities.

The influence of energy losses on the angular distribution of protons can be traced in Fig. 2, where mean deflection angle of protons with observed energies  $E_f$  is shown as function of traveled distance  $r$ . As it is seen from Fig. 1, protons with energy smaller than  $E = 6 \times 10^{19}$  eV do not suffer noticeable energy losses over the distances  $\sim 100$  Mpc. In this case the diffusion in angular space can be treated as a homogeneous random walk that brings us to the dependence of the mean deflection angle on the travel distance  $\propto r^{1/2}$ . For protons with initial energy higher than the threshold of photomeson production, the energy of protons gradually decreases which leads to deviation from this simple dependence. In particular, for the given *observed* (final) energy  $E_f$ , this effect implies higher original energies, and consequently smaller deflection angles at the initial parts of propagation. This results in a weaker increase of the mean deflection angle with the traveled distance in comparison with loss-free case. This effect is clearly seen from analytical expressions, which is possible to obtain in the case of constant energy loss rate

<sup>1</sup>Note that in Ref. [17], the photoproduction cross sections from the SOPHIA code [21] have been used for calculations of the differential and integral characteristics of  $p\gamma$  interactions.

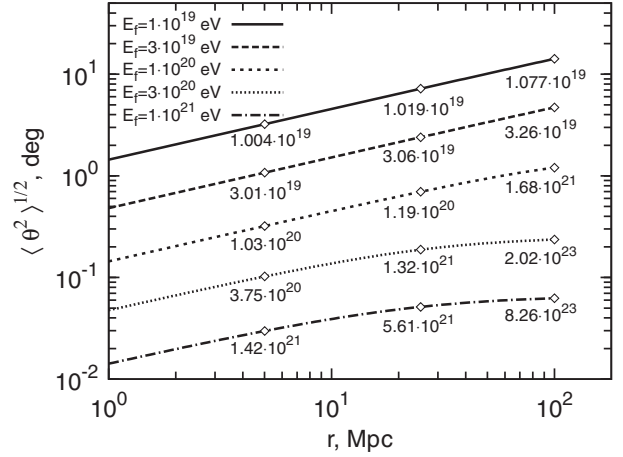


FIG. 2. The mean deflection angle of protons for the fixed *observed* energy  $E_f$  over the distance  $r$ . The numbers at the curves indicate the energies which proton had at the distance  $r$  from the observer.

$$\left| \frac{dE}{dz} \right| \frac{1}{E} = b = \text{const:}$$

$$\langle \theta^2 \rangle \sim \frac{r}{E_f^2} \left( \frac{\xi^2 - 2\xi + 2(1 - e^{-\xi})}{\xi^3} \right) \Big|_{\xi=2br}. \quad (47)$$

Expanding this expression into series in terms of powers of  $r$  we obtain:

$$\langle \theta^2 \rangle \sim \frac{1}{E_f^2} \left( \frac{r}{3} - \frac{br^2}{6} + \dots \right). \quad (48)$$

The first term does not depend on the value of  $b$  and thereby describes the loss-free propagation. The next term takes into account the energy losses and makes the dependence on the distance  $r$  weaker. While Eq. (47) approximately describes the behavior of mean deflection angle for the final energy  $E_f \geq 10^{21}$  eV, the first term of Eq. (48) describes the case of  $E_f \leq 6 \times 10^{19}$  eV. In Fig. 2 the mean deflection angle of protons is given for IGMF  $B = 1$  nG. Since the dependence of the average deflection angle on the magnetic field is linear, it is easy to produce plots for other magnetic fields.

In order to indicate the evolution of the energy of protons during their propagation through the 2.7 K CMBR, in Fig. 2 we indicate at the corresponding curves, calculated for the fixed observed (final) energies of protons, the energies which protons had at different distances from the observer. For the fixed observed energies exceeding the threshold of photomeson production, the calculated initial energies grow dramatically with the increase of the distance, especially for  $\geq 100$  Mpc. Therefore, any deficit of protons of such high energies in the initial spectrum would result in the cutoff in the observed spectrum at the corresponding energies.

The energy distributions of protons at distances 100 Mpc and 300 Mpc are shown in Fig. 3 for the initial differential

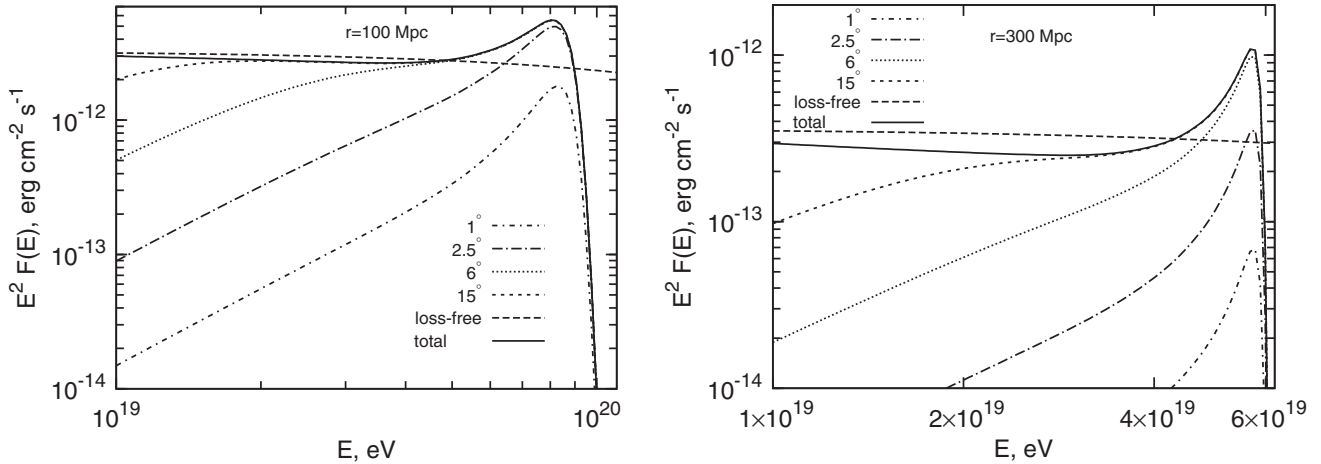


FIG. 3. Energy flux distribution of protons observed within different angles for the source at the distance  $r = 100$  Mpc (left panel) and  $r = 300$  Mpc (right panel). The initial spectrum of protons is assumed power-law with an exponential cutoff at  $E_0 = 3 \times 10^{20}$  eV, the IGMF is 1 nG.

energy spectrum  $J_p(E) = J_0 E^{-2} \exp(-E/E_0)$ . The total luminosity of the source in CRs with energy above  $10^9$  eV is taken  $L = 10^{44}$  erg/s. The upper dashed lines correspond to the case when protons propagate in empty space; flux is determined by the geometrical factor  $1/r^2$ . Solid line presents the case when the deflections in the magnetic field are ignored. Comparison of these two curves reveals two features: a bump and a sagging at lower energies. Both features become more prominent with increasing of the distance. The bump preceding the cutoff appears due to strong growth of energy losses at the threshold of photomeson production (see Fig. 1) that makes particles to be accumulated in this energy region; the sagging is a consequence of the energy losses due to the electron-positron pair production.

The approximation of continuous energy losses takes into consideration the mean energy losses. In general it provides an acceptable accuracy but some features connected with stochastic properties of interactions should be taken into account for precise description of the spectrum in the cutoff region. The fluctuations in the energy losses do have an impact on the form of the bump and the cutoff in the observed spectrum of protons. It results, in particular, in a smoother cutoff and a broader and lower-amplitude bump [20,22] compared to the results calculated within the continuous energy losses approximation.

The bump characterizes the energy spectra of protons from discrete sources; in the case of diffuse spectra the bump disappears (see e.g. Ref. [20]). Note that the diffuse spectrum can be formed not only in the case of superposition of contributions from sources distributed in space, but also in the scenario of a single source when the IGMF are strong enough to fully isotropized the flux of protons. On the other hand, in the case of moderate intergalactic magnetic fields ( $B \sim 10^{-9} - 10^{-7}$  G) and a certain distance to the source, when the protons are deflected selectively,

depending on their energy, one should expect a much more prominent maximum at highest energies compared to the “photoproduction energy loss bump.” Indeed, the scattering in the magnetic field leads to strong dependence of the energy distribution on the solid angle within which the particles are detected. Consequently, the flux of protons at highest energies is concentrated along the direction to the source. This is demonstrated in Fig. 3.

### B. Electrons

The secondary gamma rays and neutrinos are tracers of propagation of protons in the IGM. The first generation gamma rays from photomeson processes are produced at extremely high energies  $E \geq 10^{19}$  eV. They are effectively absorbed due to interactions with the photons of CMBR and the cosmic radio background (CRB) over distance  $\sim 1$  Mpc. Because of the threshold effects, at energies below  $10^{14}$  eV the efficiency of interactions with CMBR dramatically drops, but gamma rays continue to interact with the infrared and optical photons of the EBL. At these energies the mean three path of gamma rays increases sharply achieving,  $\sim 100$  Mpc at  $E_\gamma \sim 10$  TeV, and  $\sim 1$  Gpc at  $E \leq 200$  GeV (see, e.g., Ref. [23]). Thus, as long as we are interested in gamma rays from the sources of highest energy cosmic rays, the energy of gamma rays should not significantly exceed 1 TeV. In this energy band gamma rays are produced through the electromagnetic cascade initiated by the products of decays of short-lived mesons from the photomeson interactions and, partly, by electrons from the Bethe-Heitler pair-production process. For the development of an effective cascade the magnetic field should be smaller than  $10^{-10}$  G. Even so, the observer can see the cascade gamma rays in the direction of the source only in the case of extremely small IGMF,  $B \leq 10^{-15}$  G. A collimated beam of gamma rays of GeV–TeV energies is expected in the case of magnetized IGM with



$B \geq 10^{-9}$  G. These gamma rays are produced through the synchrotron radiation of  $E \geq 10^{19}$  eV electrons.

Because of very large Lorentz factor of particles, we can assume that secondary products from all interactions under consideration propagate strictly in the direction of the parent particle. Therefore observed angular distribution of gamma rays depends on the influence of IGMF on electrons that produce these gamma rays. To observe the UHECR source in gamma rays it is necessary that producing electrons are only slightly deflected in IGMF.

The almost rectilinear part of the path of electrons is much smaller than distances traveled by protons and is comparable to the typical correlation length,  $\lambda \approx 1$  Mpc. So the scattering of electrons takes place in an almost homogeneous magnetic field. But since the direction of magnetic field has a random character, the scattering occurs in random directions. In the case of electrons, one can apply the formalism of the multiple scattering to the random single scattering. Indeed, as has been noted the distribution function should be a smooth function of angle to write the elastic collision integral in the Fokker-Planck approximation. If all particles are scattered, as in the case of electrons, the distribution function does not include a part with sharp angular distribution corresponding to non-scattered particles.

To obtain the mean square deflection angle per unit length, we introduce a new parameter, namely, the electron deflection angle resulting from the propagation while the electron energy is reduced from the initial value of  $E'$  to  $E$ :

$$\theta = \int_E^{E'} \frac{1}{\bar{\epsilon}_e r_g} dE'', \quad (49)$$

where  $\bar{\epsilon}_e$  is rate of energy losses due to synchrotron radiation and  $r_g$  is gyroradius. Taking into account random field orientations we find

$$\langle \theta_s^2 \rangle = \frac{3}{2} \frac{(mc^2)^4}{e^2 E} \left( \frac{1}{E} - \frac{1}{E'} \right) \left( \frac{1}{E} + \frac{2}{3} \frac{1}{E'} \right). \quad (50)$$

After substituting this equation into Eq. (5) we find the coefficients  $A_{ei}$  of the diffusion coefficient  $D_e$  in simple analytical forms:

$$A_1 = \frac{5\alpha\beta}{180} \frac{1}{E^4} (7\xi^2 + 14\xi + 9)(1 - \xi)^2, \quad (51)$$

$$A_2 = \frac{\alpha\beta^2}{180} \frac{1}{E^5} (19\xi^2 + 22\xi + 9)(1 - \xi)^3, \quad (52)$$

$$A_3 = \frac{\alpha\beta^3}{180} \frac{1}{E^6} (12\xi^2 + 10\xi + 3)(1 - \xi)^4, \quad (53)$$

where

$$\alpha = \frac{6}{5} \frac{(mc^2)^4}{e^2}, \quad \beta = \frac{9}{4} \frac{(mc^2)^4}{e^4 B^2}, \quad \xi = \frac{E}{E'}. \quad (54)$$

Equation (49) can be written in the form

$$\theta \approx 0.008^\circ \frac{(1 - \xi^2)}{B_{\text{nG}} E_{20}^2}, \quad (55)$$

where  $B_{\text{nG}}$  is the magnetic field in units of nano Gauss (nG),  $E_{20}$  is final energy in units of  $10^{20}$  eV,  $\xi = E/E'$ . Here the random orientations of the field are taken into account. This expression allows us to estimate the threshold of isotropization. Indeed, if the electron loses a considerable part of its energy, then  $\xi \ll 1$  and the deflection angle mostly depends on the final energy. The deflection angle becomes quite large ( $\sim 1$  radian) in the magnetic field 1 nG when final energy is  $E \approx 2 \times 10^{18}$  eV. For greater magnetic field, the threshold of isotropization is shifted to the range of lower energies. It should be noted that for magnetic fields 1–100 nG this threshold appears in the energy region where the energy losses due to synchrotron radiation dominate over the inverse Compton scattering (see Fig. 4).

It means that inverse Compton scattering can be neglected for electrons under consideration.

Let us estimate the energy of gamma rays produced by electrons with energy exceeding the threshold of isotropization. Using modified Eq. (D1) for energy distribution of synchrotron radiation in chaotic magnetic fields, we find the energies of electrons that produce synchrotron gamma rays with energy  $E_\gamma$ :

$$E_e = 1.23 \times 10^{14} \sqrt{\frac{E_\gamma}{xB_{\text{nG}}}}. \quad (56)$$

Here  $E_e$  and  $E_\gamma$  are given in units of eV,  $x$  is the dimensionless argument of distribution function Eq. (D5). The latter has a maximum at  $x \approx 0.2291$  and exponentially decreases for large  $x$  [see Eq. (D7)]. To make sure that

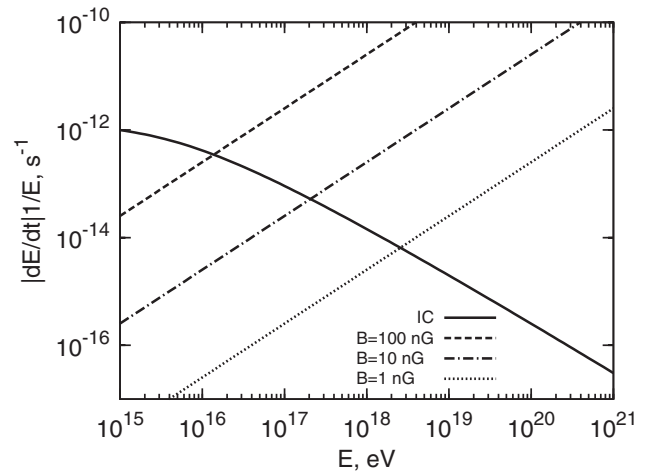


FIG. 4. Energy loss rates of electrons due to inverse Compton scattering on CMBR photons (solid line) and synchrotron radiation in random magnetic field for  $B = 1$  nG, 10 nG, and 100 nG. For electrons of energy  $E \geq 10^{19}$  eV the inverse Compton scattering on the radio waves of CRB becomes comparable or even can exceed the contribution of the Compton scattering on CMBR, however for IGMF  $B \geq 1$  nG the synchrotron radiation remains the main cooling channel.

observed gamma rays are produced by electrons with energies greater threshold of isotropization we should consider gamma rays with energies  $E_\gamma \gtrsim 10^9$  eV. Indeed, electrons with energies corresponding to  $x \gtrsim 10$  in the Eq. (56) give exponentially small contribution into radiation of gamma rays of the given energy. Therefore, assuming  $x = 10$ , we find that the contribution of electrons with energies below threshold of isotropization  $E_e \lesssim 10^{18}$  eV into radiation of  $E_\gamma = 10^9$  eV gamma rays is insignificant. According to Eq. (55) the product  $BE^2$  is constant for the isotropization threshold. Since the same combination enters in Eq. (56) the minimal energy of gamma rays produced by the electrons under consideration does not depend on the magnetic field.

At interactions of protons with the intergalactic radiation fields the ultrahigh energy electrons are produced via two channels: pair production and photomeson production processes. In the pair production process only a small ( $\leq 2m_e/m_p$ ) fraction of proton energy is converted to the secondary electrons. For the magnetic field of order of nG or larger, the energies of these electrons appear below the threshold of isotropization, thus they do not contribute to the gamma-ray emission emitted towards the observer. The photomeson processes lead to several nonstable secondary particles, such as  $\pi$ ,  $\eta$ ,  $K$  mesons, which decay into high energy gamma rays, neutrinos, and electrons. The electrons from the decays of these mesons are produced with energies [17] exceeding the isotropization threshold.

In addition, a significant fraction of electrons is created at interactions of the first generation ("photomeson") gamma rays with photons of CMBR and CRB. For the model of CRB suggested by [24], the mean free path of gamma rays of  $E \gtrsim 10^{19}$  eV is determined by the interactions with MHz radio waves; it is of order of several Mpc. Here we neglect by the interaction length assuming that gamma rays interact with CRB immediately after their creation. In this case the particle gets additional deflection since it is treated as an electron all along. It results in broader angular distribution of observed gamma ray in comparison with exact consideration. The interaction of gamma rays with CRB photons of energy  $\epsilon_R$  occurs in the regime  $\epsilon_R E_\gamma / m_e^2 c^4 \gg 1$ . It means that the most of the energy is converted to one of the two electrons. The energy of gamma rays is higher than the energy of electrons produced in the decays of mesons (see, e.g., Ref. [17]). Therefore electrons created by pair production process are more energetic than electrons generated in the decays of nonstable products of photomeson processes. Consequently, the pair-produced electrons result in higher flux of synchrotron radiation than the direct ones from the meson decays.

### C. Gamma rays and neutrinos

The apparent angular size of the synchrotron gamma-ray source depends on the linear size of the emitter itself and

the deflection angles of the parent electrons. Both are defined by spatial and angular distributions of electrons, respectively. In the case of spherically symmetric source and small deflection angles of electrons  $\theta_{\text{def}}$ , the source located at the distance  $r$  with the gamma-ray emission region of radius  $d$ , has an angular size  $\vartheta_{\text{obs}} \sim 2 \frac{d}{r} \theta_{\text{def}}$ . The case of an isotropically emitted gamma-ray source corresponds to  $\theta_{\text{def}} \sim 1$ . The linear size of the gamma-ray emitter can be evaluated from Fig. 5, where is shown the number of electrons of energy  $E_e$  located inside the sphere of radius  $r$ . The saturation that takes place at large distances shows the absence of electrons in this region. One can see from Fig. 5 that the size of the sphere, where the electrons are located, decreases while the energy increases. This is explained by the fact that protons producing electrons of such high energies disappear due to energy losses. For energies below  $E_e = 10^{19}$  eV the electrons are not located in a definite region. The electrons with energy below the thermalization threshold form an extended halo. These electrons have energies at which the inverse Compton scattering losses dominates over the energy losses due to the synchrotron radiation. They initiate electromagnetic cascades in the CMBR and EBL photon fields that eventually results in a very extended GeV-TeV gamma-ray emission.

The spectral energy distributions (SED) of gamma rays,  $E^2 F(E)$ , received within different angles are presented in Fig. 6. The fluxes are calculated for the same initial proton energy distribution used in Fig. 3. Three series of curves for each of two distances (left and right panels) correspond to different cutoff energies in the initial proton spectrum. One can see that the cutoff energy has significant impact on the flux of gamma rays; it increases the flux, shifts the maximum of SED towards higher energies, and makes narrower the angular distributions. These features have a simple explanation. The increase of the cutoff energy provides more secondary electrons and extends the spectrum of

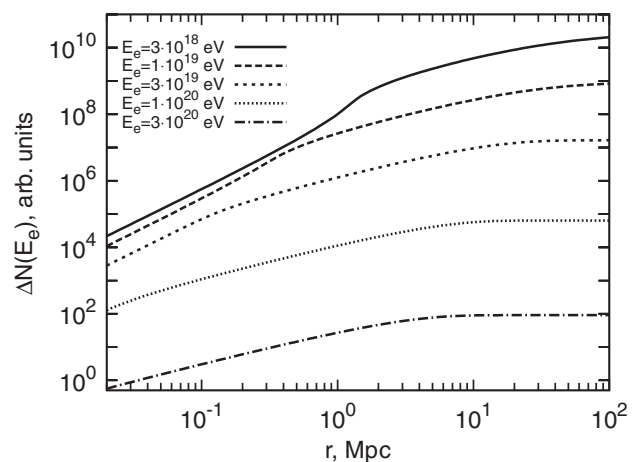


FIG. 5. Number of electrons of energy  $E_e$  located inside a sphere of the radius  $r$ .

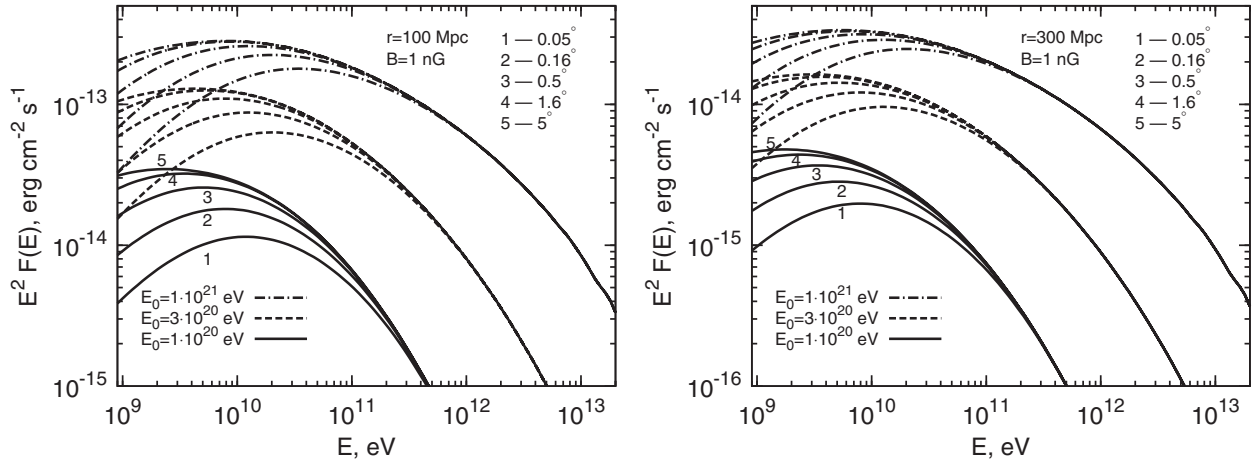


FIG. 6. Flux distributions of gamma rays observed within different angles in the direction of the source located at the distance  $r = 100$  Mpc (left panel) and  $r = 300$  Mpc (right panel). Calculations correspond to the IGMF  $B = 1$  nG and initial power-law distributions of protons with spectral index  $\alpha = 2$  and exponential cutoffs at  $E_0 = 10^{20}$  eV;  $3 \times 10^{20}$  eV, and  $10^{21}$  eV. The total power of injection of protons into IGM is  $10^{44}$  erg/s.

electrons to more energetic region. The latter leads to smaller deflections. It is interesting to note that although the angular distribution of gamma rays is composed of deflections of both protons and electrons, their angular distribution is more narrow compared to the angular distribution of protons (see, Fig. 3). This is explained by the fact that the main portion of gamma rays is produced in regions close to the source by the highest energy protons which did not suffer significant energy losses (see, Fig. 5), while the multiple scattering in IGMF contributes to the formation of the angular distribution of protons over the entire path from the source to the observer. Since the angular size of the gamma-ray source is determined by the geometrical factor  $d/r$ , the distribution of gamma rays from a source at the distance  $r = 300$  Mpc is narrower than from an identical source located at the distance  $r = 100$  Mpc. It is remarkable that at very high energies the source becomes pointlike. In particular, at energies above  $E_\gamma \approx 5 \times 10^{11}$  eV, the observer will see the gamma-ray source located at the distance of 100 Mpc within an angle smaller than  $\theta_{\text{obs}} = 0.1^\circ$ .

Figure 7 shows the impact of the IGMF strength on the flux distribution of gamma rays. The increase of the magnetic field leads to the shift of the maximum of SED to higher energies. In accordance with Eq. (56), the shift of the synchrotron peak is proportional to the strength of the magnetic field since the energy distribution of electrons does not depend on the magnetic field. Finally, note that the increase of the magnetic field implies strong deflections which leads to the reduction of the flux and widening of the angular distribution of gamma rays.

For the sources located beyond 100 Mpc, TeV gamma rays interact effectively with optical and infrared photons of the EBL. The energy-dependent absorption of gamma rays is characterized by the optical depth  $\tau_{\gamma\gamma}$  which depends on the EBL flux and is proportional to the distance to

the source. Unfortunately the EBL flux contains quite large uncertainties, especially at the mid and far IR wavelengths which are most relevant to the gamma-ray energy band and the source distances discussed in this paper. The impact of these uncertainties on the intergalactic absorption of gamma rays is discussed in Ref. [23]. Even for the minimum EBL flux at infrared wavelengths, the absorption of TeV gamma rays from sources beyond 100 Mpc can be significant; at multi-TeV energies the optical depth  $\tau_{\gamma\gamma}$  exceed 1. Therefore, the curves in Figs. 6–8 should be

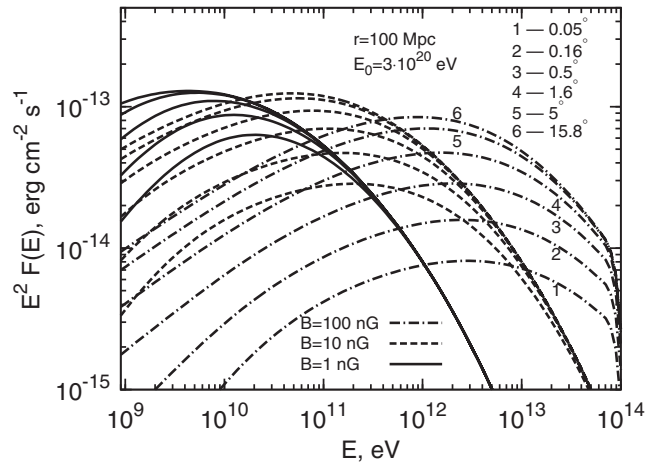


FIG. 7. Flux distributions of gamma rays observed within different angles in the direction of the cosmic ray source at the distance  $r = 100$  Mpc. The calculations are performed for three different IGMF  $B = 1$  nG, 10 nG, 100 nG, assuming an initial power-law distribution of protons with spectral index  $\alpha = 2$  an exponential cutoff at  $E_0 = 3 \times 10^{20}$  eV. The total power of injection of protons into IGM is  $10^{44}$  erg/s. The intergalactic absorption of gamma rays due to interactions with EBL is not taken into account.

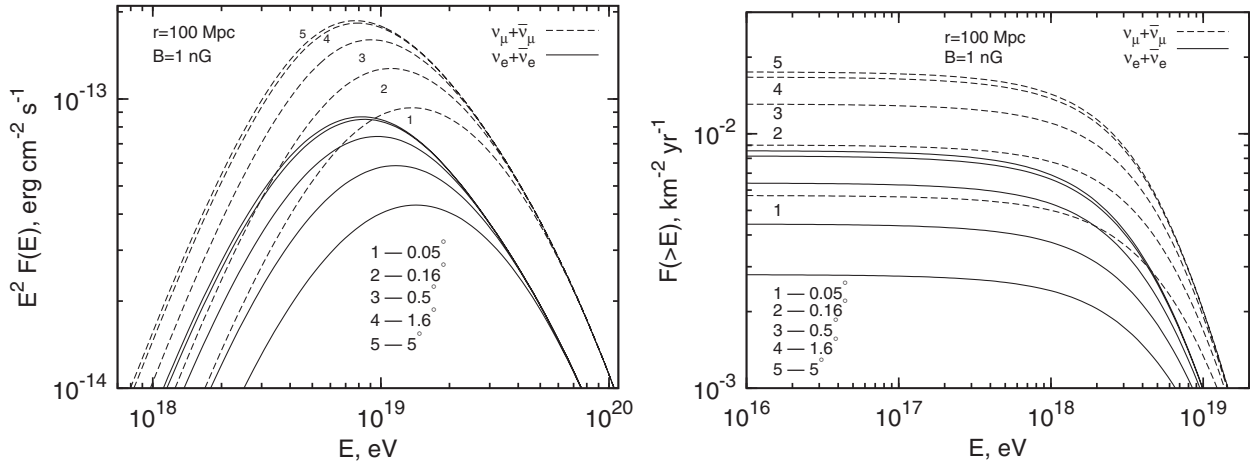


FIG. 8. The fluxes of neutrinos observed within different angles in the direction of the cosmic ray proton source located at the distance  $r = 100$  Mpc. The calculations are performed for the initial power-law distribution of protons with spectral index  $\alpha = 2$  and the exponential cutoff at  $E_0 = 3 \times 10^{20}$  eV. The IGMF  $B = 1$  nG, and the total power of injection of protons into IGM is  $10^{44}$  erg/s. Left panel is spectral energy distributions, right panel is integral fluxes.

corrected by multiplying the unabsorbed fluxes to the factor  $\exp(-\tau_{\gamma\gamma})$ .

The decay of nonstable products of photomeson processes leads to the appearance of extremely high energy electrons (positrons) and neutrinos (antineutrinos). Since the magnetic field does not have an impact on neutrinos, the angular distribution of neutrinos is determined only by the deflection of protons. This leads to more narrow angular distributions of neutrinos compared not only to the distributions of protons (for the same reason described above for gamma rays) but also compared to the distribution of gamma rays (because the gamma-ray distribution is additionally broadened due to deflections of electrons). The left panel of Fig. 8 shows SED of neutrinos and

antineutrinos received within different angles. The right panel of the figure presents the integral fluxes of neutrinos. The impact of the cutoff energy in the initial proton spectrum on the neutrino flux is demonstrated in Fig. 9.

For comparison, the spectral energy distributions of protons, gamma rays and muon neutrinos are shown together in Figs. 10 and 11 for two distance to the source—30 Mpc and 300 Mpc.

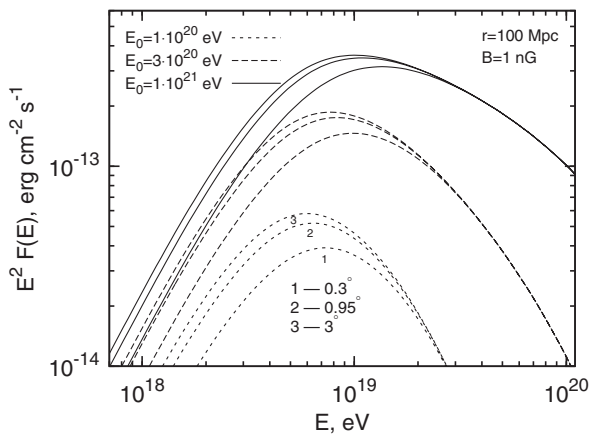


FIG. 9. The spectral energy distributions of muon neutrinos observed within different angles towards the source of cosmic ray protons located at  $r = 100$  Mpc. The calculations are performed for initial power-law distribution of protons with  $\alpha = 2$  and three different values of the exponential cutoff:  $E_0 = 10^{20}$  eV,  $3 \times 10^{20}$  eV, and  $10^{21}$  eV.

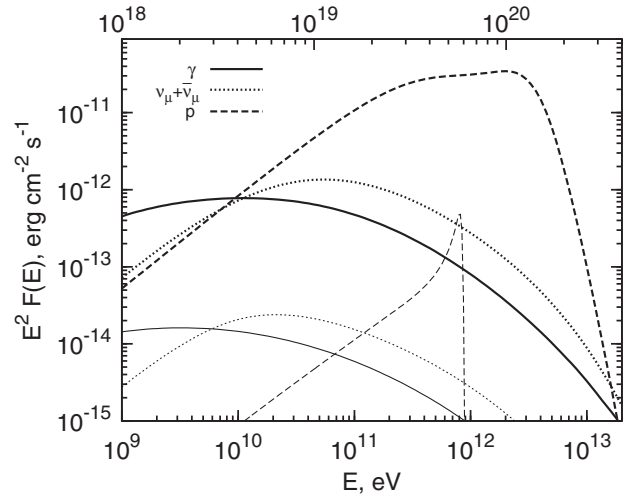


FIG. 10. The spectral energy distributions of gamma rays, muon neutrinos, and protons observed within the polar angle  $3^\circ$  from two identical source located at  $r = 30$  Mpc (thick lines) and  $r = 300$  Mpc (thin lines). The upper energy scale is for protons and neutrinos, the lower energy scale is for gamma rays. The calculations are performed for the initial power-law distribution of protons with spectral index  $\alpha = 2$ , the exponential cutoff  $E_0 = 3 \times 10^{20}$  eV, and the total power of injection into IGM  $10^{44}$  erg/s. The IGMF is 1 nG.

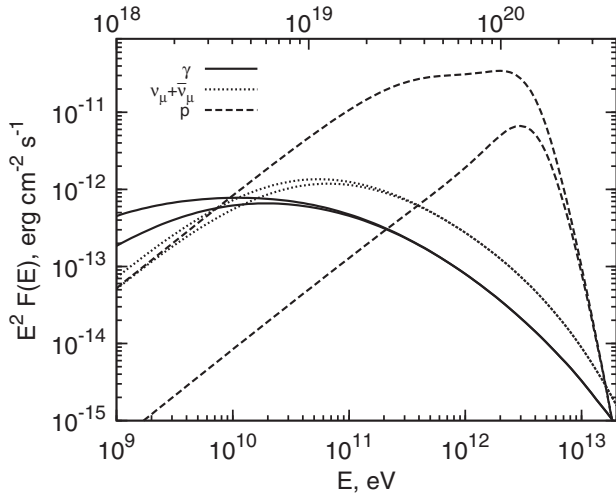


FIG. 11. The spectral energy distribution of gamma rays, muon neutrinos, and protons observed within polar angles  $0.3^\circ$  and  $3^\circ$  towards a source located at  $r = 30$  Mpc. The parameters for the IGMF and the proton spectrum are the same as in Fig. 10.

#### IV. AN IMPULSIVE SOURCE: ARRIVAL-TIME DISTRIBUTIONS

Let us assume that at the moment  $t = 0$  an impulsive spherically-symmetric source injects protons into the IGM. The multiple scattering of protons in the chaotic magnetic field results in the deviation of the motion of particles from the rectilinear propagation, therefore they arrive to the observer with significant time delays. The arrival time of the proton moving with a speed  $v_p$  over the path  $S$  is

$$t = \frac{S}{v_p} = \frac{S}{c} + 4.5 \times 10^{-4} \left( \frac{S_{\text{Mpc}}}{100} \right) \left( \frac{10^{18}}{E_{\text{eV}}} \right)^2 \text{ s}. \quad (57)$$

For ultrarelativistic protons the second term is negligible, therefore in calculations we adopt  $v_p = c$ . In this paper we will study the distribution of the arrival-time delays  $\tau = t - r/c$  ignoring the energy losses of particles.

Let us denote by  $P(\tau, \zeta, r)d\zeta d\tau$  the probability that the proton with arrival direction in the interval  $(\zeta, \zeta + d\zeta)$  is detected at the distance  $r$  from the source in the time interval  $(\tau, \tau + d\tau)$ . Here  $\zeta = \theta^2$ , where  $\theta$  is the angle between the proton direction at the point  $\mathbf{r}$  and the vector  $\mathbf{r}$ . It is assumed that  $P$  satisfies to the condition of normalization given by Eq. (C27). The equation for the function  $P$  for a pulse of radiation in the small-angle approximation is obtained in Ref. [25]. In Appendix C we derive the exact relation between  $P$  and the standard distribution function  $f$ , and obtain  $P$  in a quite different (simpler) way than in Ref. [25]. Namely, our treatment of the problem is based on the solution of equations written for the standard distribution function.

Following Ref. [25], we introduce the function  $G$  which is determined from the equation

$$P(\tau, \zeta, r) = \frac{c}{r^3 \langle \theta_s^2 \rangle^2} G(x, y), \quad (58)$$

where the dimensionless parameters  $x$  and  $y$  are

$$x = \frac{\zeta}{r \langle \theta_s^2 \rangle} = \frac{\theta^2}{r \langle \theta_s^2 \rangle}, \quad y = \frac{c\tau}{r^2 \langle \theta_s^2 \rangle}. \quad (59)$$

Function  $G$  can be presented in the form of the one-dimensional integral

$$G(x, y) = \int_{-\infty}^{\infty} \frac{ds}{2\pi} \tilde{G}(x, s) e^{isy}. \quad (60)$$

Here

$$\tilde{G}(x, s) = \frac{z}{j_1(z)} \exp\left(-x \frac{z j_0(z)}{j_1(z)}\right), \quad (61)$$

where  $z = \sqrt{s/(2i)}$ ,  $j_0$  and  $j_1$  are spherical Bessel functions:

$$j_0(z) = \frac{\sin z}{z}, \quad j_1(z) = \frac{\sin z}{z^2} - \frac{\cos z}{z}. \quad (62)$$

The angular distribution of particles changes with time. It can be shown, by using Eqs. (60) and (61), that

$$\langle \theta^2 \rangle(\tau) = 4c\tau/r, \quad (63)$$

where

$$\langle \theta^2 \rangle(\tau) = \int_0^\infty \theta^2 G(x, y) dx / \int_0^\infty G(x, y) dx \quad (64)$$

is the mean square deflection angle at the moment  $\tau$ . Quite remarkably no model parameters enter in (63) in an explicit form. Thus, the measurements of  $\theta^2$  at different time periods allow an estimate of the distance to the source. This is a nice feature, because it could be the only channel of information about the distance to the source, if the latter is not active anymore.

From Eqs. (60) and (61) follows that  $G(x, y) = 0$  at  $y < 0$ . We should note also the useful relation

$$\tilde{G}(x, s) = \int_{-\infty}^{\infty} dy G(x, y) e^{-isy}, \quad (65)$$

which allows us to obtain the moments of the function  $G$ :

$$m_n \equiv \int_{-\infty}^{\infty} dy y^n G(x, y) = i^n \frac{\partial^n}{\partial s^n} \tilde{G}(x, s) |_{s=0}. \quad (66)$$

Let us write down the first three moments:

$$m_0 = 3e^{-3x}, \quad (67)$$

$$m_1 = \frac{3}{20}(1 + 2x)e^{-3x}, \quad (68)$$

$$m_2 = \frac{3}{2800}(9 + 36x + 28x^2)e^{-3x}. \quad (69)$$

Correspondingly the mean values for  $\langle y \rangle$  and  $\langle y^2 \rangle$  are

$$\langle y \rangle = \frac{m_1}{m_0} = \frac{1}{20}(1 + 2x), \quad (70)$$

$$\langle y^2 \rangle = \frac{m_2}{m_0} = \frac{1}{100} \left( \frac{9}{28} + \frac{9}{7}x + x^2 \right). \quad (71)$$

For the dispersion of distribution  $\Delta$  and the ratio  $\frac{\Delta}{\langle y^2 \rangle}$  we have

$$\Delta \equiv \langle y^2 \rangle - \langle y \rangle^2 = \frac{1}{1400}(1 + 4x), \quad (72)$$

and

$$\frac{\Delta}{\langle y^2 \rangle} = \frac{2}{7} \frac{1 + 4x}{(1 + 2x)^2} \leq \frac{2}{7}. \quad (73)$$

This implies that we deal with a rather narrow distribution. Rewriting Eq. (70) in the form

$$\frac{c\langle \tau \rangle}{r^2 \langle \theta_s^2 \rangle} = \frac{1}{20} \left( 1 + \frac{2\theta^2}{r\langle \theta_s^2 \rangle} \right) \quad (74)$$

one can see that the measurement of  $\langle \tau \rangle$  for the particles with different values of  $\theta$  allows us to estimate  $\langle \theta_s^2 \rangle$ .

Below we discuss two special cases of practical interest.

A. Detection of protons with arbitrary arrival angles. This is the case discussed in Ref. [25]. In this case the distribution over  $\tau$  is described as

$$f_A \equiv \int_0^\infty P(\tau, \zeta, r) d\zeta = \frac{4\pi^2 c}{r^3 \langle \theta_s^2 \rangle^2} \sum_{n=1}^{\infty} (-1)^{n-1} n^2 e^{-2\pi^2 n^2 y}. \quad (75)$$

with mean values for  $y$ :

$$\langle y \rangle = \frac{1}{12}, \quad \langle y^2 \rangle = \frac{7}{720}, \quad \Delta = \frac{1}{360}. \quad (76)$$

B. Protons arriving along the radius-vector at the registration point. For this case, substituting  $x = 0$  into Eq. (60), we obtain

$$f_B \equiv P(\tau, \zeta = 0, r) = -\frac{c}{r^3 \langle \theta_s^2 \rangle^2} \sum_{n=1}^{\infty} \frac{z_n^2}{j_1'(z_n)} e^{-2z_n^2 y}, \quad (77)$$

where  $0 < z_1 < z_2 < \dots$  are the zeros of the function  $j_1(z)$ , located in the region  $z > 0$ .

The functions  $f_A$  and  $f_B$  corresponding to Eqs. (75) and (77) are shown in Fig. 12.

As it follows from Eq. (58), the arrival time  $\tau$  enters into  $P$  only in the form of combination of the variable  $y$ . Since

$$\lg y = \lg \tau - 2 \lg r - \lg \lambda - 2 \lg B + 2 \lg E + \text{const}, \quad (78)$$

the curves for other values of the relevant parameters, namely, energy  $E$ , magnetic field  $B$ , correlation length  $\lambda$ , and the distance to the source  $r$ , can be obtained by a simple shift along the  $\tau$ -axis. However, it should be noted that Eq. (58) is obtained in the approximation of ignoring the energy losses of protons. Therefore for the large distances,  $r \geq 100$  Mpc, and especially for large energies,

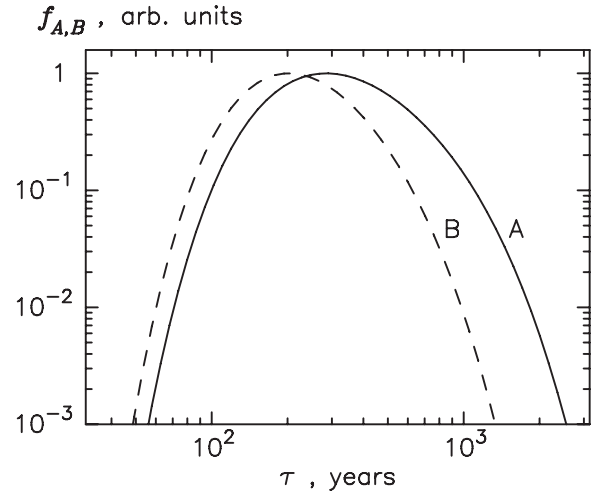


FIG. 12. The arrival-time distributions for the cases A (solid line) and B (dashed line) discussed in the text. The distance to the source is  $r = 10$  Mpc, the energy of protons  $E = 10^{20}$  eV, and the strength of the magnetic field  $B = 1$  nG. The curves are shown in arbitrary units; for convenience they are normalized to 1 at the points of the maximum of distributions:  $\max(f_{A,B}) = 1$ .

$E \geq 10^{20}$  eV, Eq. (58) overestimates the arrival time, given that the energy of protons during their propagation significantly exceeds the energy at the registration point (see Fig. 1). Therefore, for large distance Eq. (58) should be treated as an upper limit for the time delay. On the other hand, since gamma rays are produced at the very beginning of propagation of protons (within 10 Mpc or so), the curves calculated for a distance of order of 10 Mpc, provide a quite accurate estimate for the arrival times of gamma rays.

As it is seen from Fig. 12 the delays of arrival times of  $10^{20}$  eV protons as well as the secondary neutrinos and gamma rays, even from relatively nearby sources and weak intergalactic magnetic fields, are significant. The association of these particles to short solitary events like GRB with duration of 1 min or less, would be possible only if

$$\left( \frac{r}{10 \text{ Mpc}} \right) \left( \frac{B}{10^{-13} \text{ G}} \right) \lesssim 1. \quad (79)$$

## V. SUMMARY

In this paper the angular, spectral and time distributions of UHE protons and the associated secondary gamma rays and neutrinos propagating through the intergalactic radiation and magnetic fields have been studied based on the relevant solutions of the Boltzmann transport equation in the small-angle and continuous energy loss approximations. A general formalism for the treatment of the steady-state distributions is provided in the form of relatively simple analytical presentations. The treatment of the secondary products, in particular, the synchrotron gamma-radiation of electrons from photomeson interactions is reduced to the consecutive application of the solutions

which schematically can be presented as

$$Q_p \rightarrow f_p \rightarrow Q_e \rightarrow f_e \rightarrow Q_\gamma \rightarrow f_\gamma.$$

Here  $Q_i$  denotes a source function and  $f_i$  denotes a distribution function.  $Q_p$  is specified as spherically symmetric source of protons.  $Q_e$  is obtained from distribution function of protons as the final product of photomeson interactions using the results Ref. [17]. Electrons generated in the pair-production process of the first generation gamma rays (from the decay of neutral  $\pi$ -mesons) are also included in  $Q_e$ . Finally,  $Q_\gamma$  corresponds to the synchrotron radiation of electrons with distribution function  $f_e$  formed in the chaotic magnetic field. We consider the case of strong magnetic field,  $B \geq 10^{-9}$  G, when the electrons from photomeson interactions are cooled predominantly via synchrotron radiation. Such strong magnetic fields prevent the development of pair cascades at highest energies, and, at the same time, allow very effective conversion of the electromagnetic energy released at photomeson interactions into synchrotron radiation. The latter peaks at GeV and TeV energies. The electromagnetic cascades are developed at lower energies at which the suppression of the Compton cooling due to the Klein-Nishina effect is becoming more relaxed. These subcascades are initiated basically by the electrons-positron pairs produced at the inverse Bethe-Heitler process. However, because of deflections of low-energy electrons in chaotic IGMF, the gamma rays produced during the cascade development lose the directionality. Moreover, if the initial energy distribution of protons extends to  $10^{20}$  eV, the electromagnetic energy released in photomeson interactions greatly exceeds the energy supply from the Bethe-Heitler process. On the other hand, the synchrotron radiation produced by highest energy secondary electrons not only provides an almost 100% effective conversion into gamma rays, but also preserves the initial direction of protons as long as the magnetic field does not exceed  $10^{-7}$  G. Remarkably, while the main fraction of synchrotron gamma rays and the highest energy neutrinos is produced in the proximity of the source, namely, within the first  $\approx 10$  Mpc of the initial path of protons, the latter continue to suffer deflections with an enhanced rate (because of gradual decrease of energy during the propagation through the 2.7 CMBR), until they arrive to the observer. Therefore, the gamma-ray and neutrino distributions appear to be more narrow than the angular distribution of protons.

The distribution functions  $f_p$  and  $f_e$  are obtained by applying the Green function of transport equation to the source functions  $Q_p$  and  $Q_e$ , respectively. The angular part of  $f_p$  and  $f_e$  is a normal (Gaussian-like) distribution, the dispersion of which depends on the energy loss rate, the deflection angle per unit length and the distance to the source.  $f_\gamma$  is calculated by integration along optical depth at different angles towards the source.

For specific realizations of the scenario of small-angle deflection of charged particles, assuming that they move in a statistically isotropic and homogeneous turbulent magnetic field with Kolmogorov spectrum, we considered the IGMF in the interval from  $10^{-9}$  to  $10^{-7}$  Gauss and adopted 1 Mpc for the correlation length. The propagation of protons is considered, as long as it concerns the energy losses, as rectilinear with diffusion in angle. Transport of electrons is considered in the homogeneous magnetic field with random direction since their propagation length is of the order or less of 1 Mpc.

Despite the small-angle scatterings, the related elongation of particle trajectories causes significant delays of their arrival time. The problem of propagation of particles can be described by the steady-state solutions if the lifetime of the source exceeds the delay times. Otherwise the problem should be treated as a time-dependent propagation of particles injected in the IGM by an impulsive source of extremely high energy protons. This could be the case of solitary events like GRB or short periods ( $T \leq 10^5$  year) of enhanced activity of active galactic nuclei. In this paper we discuss the case of an impulsive source, ignoring the energy losses of protons. This approximation limits the applicability of the derived time distribution functions to the relatively nearby sources of protons located within 100 Mpc sphere of the nearby Universe. On the other hand, since the bulk of synchrotron radiation of secondary electrons is produced close the source,  $R \leq 10$  Mpc, the time-dependent solutions derived for protons, can describe quite accurately the delayed arrival times of synchrotron photons from sources located at cosmological distances.

The results presented in this paper for gamma rays are valid for IGMF in a specific (but perhaps the most realistic) range between  $B = 10^{-9}$ – $10^{-7}$  G. IGMF stronger than  $10^{-7}$  G would lead to large deflections of charged particles, and thus violate the condition of small-angle approximation. On the other hand, IGMF weaker than  $10^{-10}$  G would reduce dramatically the efficiency of the synchrotron radiation since in this case the electrons are cooled predominantly via Compton scattering. The pair cascades initiated by these electrons also lead to GeV and TeV gamma-ray emission, however these cascades form giant (hardly detectable) halos around the sources, unless the magnetic field is extremely weak, smaller than  $10^{-15}$  G.

The realization of the scenario of synchrotron radiation of secondary electrons at the presence of a relatively modest magnetic field,  $B \sim 10^{-9}$  G or larger, in the 10 Mpc proximity of the sources of highest energy cosmic rays, has higher chances to be detected, given the compact (almost pointlike) images at GeV and especially TeV energies, and the very high (10 per cent or more) efficiency of conversion of the energy of protons to high energy synchrotron gamma rays. The fluxes of gamma rays, protons, and neutrinos shown in Figs. 7–11 are obtained assuming a power-law energy spectrum of protons with  $\alpha = 2$  and

total injection rate into IGM  $L_p(\geq 1 \text{ GeV}) = 10^{44} \text{ erg/s}$ . The expected gamma-ray fluxes are close to the sensitivities of *Fermi* LAT at GeV energies and the sensitivity of the Imaging Atmospheric Cherenkov telescope arrays at TeV energies. While the total power of production of highest energy cosmic rays hardly can exceed, except for very powerful AGN,  $10^{44} \text{ erg/s}$ , in the case of blazars with small beaming angles, the expected fluxes of gamma rays could be significantly higher. Indeed, in the case of small deflections, the directions of injection of observed particles from the source are close to the observational line. Therefore, the results for the spherically symmetric source remain valid also for the narrow jet with solid angle  $\Omega_{\text{beam}} = \pi\vartheta^2$ , where  $\vartheta^2 \geq \langle\theta^2\rangle$ . Then the required power of the source (to be detected in gamma rays) is reduced by a factor  $\Omega_{\text{beam}}/4\pi$  which might be significantly small.

Finally, we should note that the calculations in this paper are performed under assumption of homogeneity of the chaotic magnetic field on scales comparable to the distance of the source. However, one might expect realizations when a significant fraction of propagation of protons takes place in regions with very low magnetic field. In fact, such voids do exist in the IGM with scales as large as 100 Mpc [26]. In these cases one has to treat the problem separately in different segments of space between the source and the observer.

### APPENDIX A: THE GREEN FUNCTION FOR SPHERICALLY SYMMETRIC SOURCE

The Green function for spherically symmetric point source is obtained by integration of Eq. (8) over all directions of the vector  $\mathbf{n}_0$ . Let us rewrite Eq. (8) in the following form:

$$G(\mathbf{r}, \mathbf{n}, \mathbf{n}_0, E, E_0) = \frac{\delta(S(E, E_0) - r)}{c\bar{\epsilon}(E)\pi^2\Delta} \exp\left(-\frac{A - \mathbf{B}\mathbf{n}_0}{\Delta}\right). \quad (\text{A1})$$

Here

$$\begin{aligned} A &= 2(A_1 r^2 - 2A_2 r + A_3) - 2A_2 r(1 - \mathbf{n}_r \mathbf{n}), \\ \mathbf{B} &= 2((A_1 r^2 - A_2 r)\mathbf{n}_r + (A_3 - A_2 r)\mathbf{n}), \end{aligned} \quad (\text{A2})$$

$$\begin{aligned} I &= \int \exp\left(-\frac{(\mathbf{n}_0 - \mathbf{n}_s)^2}{D}\right) \\ &\times \exp\left(-\frac{A_1(\mathbf{r} - \mathbf{r}_0 - |\mathbf{r} - \mathbf{r}_0|\mathbf{n}_0)^2 - 2A_2(\mathbf{r} - \mathbf{r}_0 - |\mathbf{r} - \mathbf{r}_0|\mathbf{n}_0)(\mathbf{n} - \mathbf{n}_0) + A_3(\mathbf{n} - \mathbf{n}_0)^2}{\Delta}\right) d\Omega_{\mathbf{n}_s} d\Omega_{\mathbf{n}_0}, \end{aligned} \quad (\text{B2})$$

where

$$\mathbf{r} = r\mathbf{n}_r, \quad \mathbf{r}_0 = r_0\mathbf{n}_s, \quad \mathbf{r} - \mathbf{r}_0 = r'\mathbf{n}_0, \quad (\text{B3})$$

$\Delta$  and  $D$  are defined in Eqs. (4) and (14), respectively. Taking into account that all directions are close, the inte-

gral can be presented in the following form:

$$\mathbf{B}\mathbf{n}_0 = |\mathbf{B}| \cos\theta_0 \approx |\mathbf{B}|\left(1 - \frac{\theta_0^2}{2}\right). \quad (\text{A3})$$

Performing integration by saddle point method we obtain:

$$\int \exp\left(-\frac{A - \mathbf{B}\mathbf{n}_0}{\Delta}\right) d\Omega_{\mathbf{n}_0} \approx \frac{2\pi\Delta}{|\mathbf{B}|} \exp\left(-\frac{A - |\mathbf{B}|}{\Delta}\right). \quad (\text{A4})$$

Taking into account

$$\mathbf{n}_r \mathbf{n} \approx 1 - \frac{\theta^2}{2}, \quad (\text{A5})$$

the expressions for  $A$  and  $|\mathbf{B}|$  can be written:

$$A = 2Dr^2 + \theta^2 A_2 r, \quad (\text{A6})$$

$$|\mathbf{B}| = 2\sqrt{(Dr^2)^2 - \theta^2(A_1 r^2 - A_2 r)(A_3 - A_2 r)}$$

where

$$D = A_1 - 2\frac{A_2}{r} + \frac{A_3}{r^2}. \quad (\text{A7})$$

Expanding  $|\mathbf{B}|$  into series in terms of  $\theta$  to the second-order term in exponent and retaining the first term in denominator we find

$$G_{\text{sph}}(r, \theta, E, E_0) = \frac{\delta(S(E, E_0) - r)}{c\bar{\epsilon}(E)r^2\pi D} \exp\left(-\frac{\theta^2}{D}\right). \quad (\text{A8})$$

### APPENDIX B: DISTRIBUTION FUNCTION OF ELECTRONS

After changing the order of integration in

$$\begin{aligned} f_e(\mathbf{r}, \mathbf{n}, E_e) &= \int \hat{Q}_e(f_p(\mathbf{r}_0, \mathbf{n}_0, E_p))G(\mathbf{r} \\ &- \mathbf{r}_0, \mathbf{n}, \mathbf{n}_0, E_e, E_0) d\mathbf{r}_0 \Omega_{\mathbf{n}_0} dE_{e0} \end{aligned} \quad (\text{B1})$$

we arrive at the following integral over directions of the emission of electrons  $\mathbf{n}_0$  at the point  $\mathbf{r}_0$  and directions of  $\mathbf{r}_0$ :

gral can be presented in the following form:

$$I = \int e^{-(A - \mathbf{B}\mathbf{n}_s)} d\Omega_{\mathbf{n}_s} d\Omega_{\mathbf{n}_0}, \quad (\text{B4})$$

where



$$A = X_0 + X_1(1 - \mathbf{n}_r \mathbf{n}_0) + X_2(1 - \mathbf{n}_r \mathbf{n}) + X_3(1 - \mathbf{n}_0 \mathbf{n}),$$

$$\mathbf{B} = Y_1 \mathbf{n}_0 + Y_2 \mathbf{n} + Y_3 \mathbf{n}_r. \quad (\text{B5})$$

Here we introduce the following notations:

$$X_0 = \frac{2}{D} + \frac{A_1}{\Delta}((r - r')^2 + r_0^2), \quad X_1 = \frac{2}{\Delta}(A_1 r' - A_2)r,$$

$$X_2 = \frac{2}{\Delta}A_2 r, \quad X_3 = \frac{2}{\Delta}(A_3 - A_2 r'),$$

$$Y_1 = \frac{2}{D} + \frac{2}{\Delta}(A_2 - A_1 r')r_0, \quad Y_2 = -\frac{2}{\Delta}A_2 r_0,$$

$$Y_3 = \frac{2}{\Delta}A_1 r r_0. \quad (\text{B6})$$

Since directions of  $\mathbf{n}$ ,  $\mathbf{n}_0$ , and  $\mathbf{n}_r$  are close, we can expand  $|\mathbf{B}|$  into series to the first-order terms:

$$|\mathbf{B}| \approx \nu - \frac{Y_1 Y_2}{\nu}(1 - \mathbf{n}_0 \mathbf{n}) - \frac{Y_1 Y_3}{\nu}(1 - \mathbf{n}_0 \mathbf{n}_r)$$

$$- \frac{Y_2 Y_3}{\nu}(1 - \mathbf{n} \mathbf{n}_r), \quad (\text{B7})$$

where

$$\nu = Y_1 + Y_2 + Y_3. \quad (\text{B8})$$

The integration of  $I$  over  $d\Omega_{\mathbf{n}_s}$  by saddle point method gives

$$I \approx \frac{2\pi}{\nu} \int e^{-(A-|\mathbf{B}|)} d\Omega_{\mathbf{n}_0} \quad (\text{B9})$$

To perform the integration over  $d\Omega_{\mathbf{n}_0}$  by the same method, we present the expression in the exponent in the following form:

$$A - |\mathbf{B}| = \underbrace{X_0 - \nu}_{Z_0} + \underbrace{\left(X_1 + \frac{Y_1 Y_3}{\nu}\right)}_{Z_1} (1 - \mathbf{n}_0 \mathbf{n}_r)$$

$$+ \underbrace{\left(X_2 + \frac{Y_2 Y_3}{\nu}\right)}_{Z_2} (1 - \mathbf{n} \mathbf{n}_r)$$

$$+ \underbrace{\left(X_3 + \frac{Y_1 Y_2}{\nu}\right)}_{Z_3} (1 - \mathbf{n}_0 \mathbf{n})$$

$$= \underbrace{Z_0 + Z_1 + Z_3 + Z_2(1 - \mathbf{n} \mathbf{n}_r)}_{\tilde{A}}$$

$$- \underbrace{(Z_1 \mathbf{n}_r + Z_3 \mathbf{n})}_{\tilde{\mathbf{B}}} \mathbf{n}_0$$

$$= \tilde{A} - \tilde{\mathbf{B}} \mathbf{n}_0. \quad (\text{B10})$$

Expanding  $|\tilde{\mathbf{B}}|$  into series

$$|\tilde{\mathbf{B}}| \approx \mu - \frac{Z_1 Z_3}{\mu} (1 - \mathbf{n} \mathbf{n}_r), \quad (\text{B11})$$

where

$$\mu = Z_1 + Z_3 \quad (\text{B12})$$

we find

$$I \approx \frac{4\pi^2}{\nu\mu} e^{-(\tilde{A}-|\tilde{\mathbf{B}}|)}. \quad (\text{B13})$$

Making replacements of all notations by their actual values and taking into account that

$$r' \approx r - r_0, \quad (\text{B14})$$

we finally obtain

$$I = \frac{\pi^2 \Delta D}{D_e r^2 + D r_0^2} \exp\left(-\frac{\theta^2 r^2}{D_e r^2 + D r_0^2}\right), \quad (\text{B15})$$

where

$$D_e = A_1 - 2\frac{A_2}{r} + \frac{A_3}{r^2} \quad (\text{B16})$$

and  $\theta$  is the angle between  $\mathbf{n}_r$  and  $\mathbf{n}$ . The Integration over  $r_0$  in the expression for  $f_e(\mathbf{r}, \mathbf{n}, E_e)$  can be readily performed because of  $\delta$ -function.

### APPENDIX C: DISTRIBUTION OF ARRIVAL TIMES IN THE CASE OF IMPULSIVE SOURCE

In the case of spherical symmetry the proton distribution function  $f = f(t, r, \mu)$  depends on time  $t$ , distance to the source  $r$ , and the variable  $\mu = \cos\theta = (\mathbf{n}\mathbf{r})/r$ . Here  $\mathbf{n}$  is a unit vector towards the direction of the proton speed. Let us normalize  $f$  using the condition

$$\int_0^\infty dr \int_{-1}^1 d\mu r^2 f(t, r, \mu) = 1. \quad (\text{C1})$$

Then  $r^2 f(t, r, \mu) dr d\mu$  is the probability that at the moment  $t$  the proton is located in the layer  $(r, r + dr)$  and is moving in the direction within  $(\mu, \mu + d\mu)$ . Let us assume that propagation of a single particle is fixed, i.e. the radius-vector  $\mathbf{r}_0(t)$  and the direction  $\mathbf{n}_0(t)$  are certain functions of time. For this particle, the distributions over  $r$  and  $\mu$  are described by  $\delta$ -functions:

$$f_0(t, r, \mu) = \frac{1}{r^2} \delta(r - r_0(t)) \delta(\mu - \mu_0(t)), \quad (\text{C2})$$

where  $\mu_0(t) = (\mathbf{n}_0(t)\mathbf{r}_0(t))/r_0(t)$ .

By averaging Eq. (C2) over the ensemble of particles gives the distribution function  $f$ :

$$f(t, r, \mu) = \langle f_0(t, r, \mu) \rangle. \quad (\text{C3})$$

Let us assume that for each particle  $r_0(t)$  is a monotonically increasing function of time, i.e. there are no particles in the ensemble with  $\mu \leq 0$ . Then the equation  $r = r_0(t)$  has a unique solution with  $t = t_0(r)$ , and thus one can write

$$\delta(r - r_0(t)) = \frac{1}{dr_0/dt} \delta(t - t_0(r)) = \frac{1}{c\mu_0(t)} \delta(t - t_0(r)). \quad (\text{C4})$$

Since in Eq. (C2) this expression is multiplied to  $\delta(\mu - \mu_0(t))$ , in the denominator one can replace  $\mu_0(t)$  by  $\mu$  and take the factor  $1/c\mu$  out of the integral. This yields

$$\langle \delta(r - r_0(t)) \delta(\mu - \mu_0(t)) \rangle = \frac{1}{c\mu} \langle \delta(t - t_0(r)) \delta(\mu - \tilde{\mu}_0(r)) \rangle, \quad (\text{C5})$$

where  $\tilde{\mu}_0(r) = \mu_0(t_0(r))$ .

Function  $\langle \delta(t - t_0(r)) \delta(\mu - \tilde{\mu}_0(r)) \rangle$  has the meaning of the probability distribution for  $t$  and  $\mu$ . Writing  $t = \tau + r/c$ , we obtain the probability distribution for  $\tau$  and  $\mu$  at the point  $r$ :

$$P(\tau, \mu, r) = \langle \delta(\tau + r/c - t_0(r)) \delta(\mu - \tilde{\mu}_0(r)) \rangle. \quad (\text{C6})$$

From this equation follows that  $P$  satisfies the condition of normalization

$$\int_0^\infty d\tau \int_{-1}^1 d\mu P(\tau, r, \mu) = 1. \quad (\text{C7})$$

Thus we arrive at the conclusion that the functions  $P$  and  $f$  are related as

$$P(\tau, \mu, r) = c\mu r^2 f(\tau + r/c, r, \mu) \equiv c\mu r^2 f'(\tau, r, \mu). \quad (\text{C8})$$

The distribution function satisfies the equation

$$\frac{1}{c} \frac{\partial f}{\partial t} + (\mathbf{n}\nabla)f = I, \quad (\text{C9})$$

where  $I$  is the collision integral. In the case of spherical symmetry

$$(\mathbf{n}\nabla)f = \mu \frac{\partial f}{\partial r} + \frac{1 - \mu^2}{r} \frac{\partial f}{\partial \mu}. \quad (\text{C10})$$

Replacing the variables in Eq. (C9) from  $(t, r)$  to  $(\tau = t - r/c, r)$  and presenting the collision integral in the Fokker-Planck approximation, we obtain

$$\begin{aligned} & \frac{1 - \mu}{c} \frac{\partial f'}{\partial \tau} + \mu \frac{\partial f'}{\partial r} + \frac{1 - \mu^2}{r} \frac{\partial f'}{\partial \mu} \\ & = \frac{\langle \theta_s^2 \rangle}{4} \frac{\partial}{\partial \mu} \left( (1 - \mu^2) \frac{\partial f'}{\partial \mu} \right). \end{aligned} \quad (\text{C11})$$

In the case of an impulsive source and no scattering (i.e.  $\langle \theta_s^2 \rangle = 0$ ) the distribution function normalized according to Eq. (C1) is

$$f(t, r, \mu) = 2\pi \delta(\mathbf{r} - c\mathbf{n}t). \quad (\text{C12})$$

It is convenient to rewrite Eq. (C12) in the form

$$f(t, r, \mu) = \frac{1}{cr^2} \delta(t - r/c) \delta(\mu - 1). \quad (\text{C13})$$

In order to demonstrate that the generalized functions in the forms given by Eqs. (C12) and (C13) are identical, one should multiply the right parts of these equations to an arbitrary function  $h(\mathbf{r}, \mathbf{n})$  and integrate over the space coordinates and the direction of the vector  $\mathbf{n}$ . This implies that at  $\langle \theta_s^2 \rangle = 0$

$$f'(\tau, r, \mu) = \frac{1}{cr^2} \delta(\tau) \delta(\mu - 1). \quad (\text{C14})$$

It is clear, from general physical considerations, that in the limit  $r \rightarrow 0$  Eq. (C14) is valid also at  $\langle \theta_s^2 \rangle \neq 0$ . Therefore, Eq. (C14) can be treated as a boundary condition to Eq. (C11) at the point  $r = 0$ .

An analytical solution of Eq. (C11) is possible to derive in the small-angle approximation. In the case of multiple scattering, the average angle of deviation of at the distance  $r$  is of order of  $(r\langle \theta_s^2 \rangle)^{1/2}$ . Therefore, for  $r \ll 1/\langle \theta_s^2 \rangle$  one can use the small-angle approximation. Let  $\mu = 1 - \zeta/2$ , and let us denote function  $f'(\tau, r, 1 - \zeta/2)$  by  $f'(\tau, r, \zeta)$ . Assuming  $\zeta \ll 1$ , from Eq. (C11) we obtain

$$\frac{\partial f'}{\partial r} + \frac{\zeta}{2c} \frac{\partial f'}{\partial \tau} - \frac{2\zeta}{r} \frac{\partial f'}{\partial \zeta} - \langle \theta_s^2 \rangle \frac{\partial}{\partial \zeta} \left( \zeta \frac{\partial f'}{\partial \zeta} \right) = 0. \quad (\text{C15})$$

To solve Eq. (C15) we apply the Fourier transformation:

$$\tilde{f}'(\omega, r, \zeta) = \int_{-\infty}^{\infty} f'(\tau, r, \zeta) e^{-i\omega\tau} d\tau. \quad (\text{C16})$$

Function  $\tilde{f}'$  satisfies the equation

$$\frac{\partial \tilde{f}'}{\partial r} + \frac{i\omega\zeta}{2c} \tilde{f}' - \frac{2\zeta}{r} \frac{\partial \tilde{f}'}{\partial \zeta} - \langle \theta_s^2 \rangle \frac{\partial}{\partial \zeta} \left( \zeta \frac{\partial \tilde{f}'}{\partial \zeta} \right) = 0, \quad (\text{C17})$$

and the boundary condition given by Eq. (C14) becomes

$$\tilde{f}'(\omega, r, \mu) = \frac{2}{cr^2} \delta(\zeta), \quad r \rightarrow 0. \quad (\text{C18})$$

Let us search the solution in the form

$$\tilde{f}' = e^{-\zeta a(r) + b(r)}, \quad (\text{C19})$$

where the functions  $a(r)$ ,  $b(r)$  do not depend on  $\zeta$ . Substituting Eq. (C19) in Eq. (C17), we obtain the following ordinary differential equations:

$$\frac{da}{dr} = \frac{i\omega}{2c} + \frac{2}{r} a - \langle \theta_s^2 \rangle a^2, \quad (\text{C20})$$

$$\frac{db}{dr} = -\langle \theta_s^2 \rangle a. \quad (\text{C21})$$

The solution to Eq. (C20) is

$$a(r) = \frac{1}{r\langle \theta_s^2 \rangle} \frac{z j_0(z)}{j_1(z)}, \quad (\text{C22})$$

where  $z = r\sqrt{\omega\langle \theta_s^2 \rangle}/(2ic)$ . The arbitrary constant which appears in the solution is chosen requiring singularity at the point  $r = 0$ . At  $r \rightarrow 0$  the function  $a = 3/r\langle \theta_s^2 \rangle$ . The so-

lution to Eq. (C21) is

$$b(r) = \ln\left(\frac{1}{r^3} \frac{z}{j_1(z)}\right) + \text{const}, \quad (\text{C23})$$

therefore the function  $\tilde{f}'$  is defined as

$$\tilde{f}' = C \frac{1}{r^3} \frac{z}{j_1(z)} \exp\left(-\frac{\zeta}{r\langle\theta_s^2\rangle} \frac{z j_0(z)}{j_1(z)}\right). \quad (\text{C24})$$

For determination of the constant  $C$  one should use the boundary condition given by Eq. (C18). In the limit of small  $r$ , and using the relation

$$\lim_{r \rightarrow 0} \left(\frac{B}{r} e^{-\zeta B/r}\right) = \delta(\zeta), \quad (\text{C25})$$

we find

$$\tilde{f}' = C \frac{3}{r^3} \exp\left(-\frac{3\zeta}{r\langle\theta_s^2\rangle}\right) = C \frac{\langle\theta_s^2\rangle}{r^2} \delta(\zeta). \quad (\text{C26})$$

Comparing Eqs. (C18) and (C26), we obtain  $C = 2/c\langle\theta_s^2\rangle$  and then using Eq. (C8) we find  $P$ . In the small-angle approximation we can replace the factor  $\mu$  in Eq. (C8) by unity. In order to compare our results with the solution obtained in Ref. [25], we adopt  $C = 1/c\langle\theta_s^2\rangle$ , which is equivalent to the change of the condition of normalization, namely, instead of Eq. (C7) we use

$$\int_0^\infty d\tau \int_0^\infty d\zeta P(\tau, r, \zeta) = 1, \quad (\text{C27})$$

where, because of rapid convergence, the upper limit of integration over  $d\zeta$  is set infinity. In order to present the result in the form given by Eqs. (58)–(60), one should introduce, instead of the variable  $\omega$ , a new variable of integration  $s = \omega r^2 \langle\theta_s^2\rangle / c$ .

#### APPENDIX D: EMISSIVITY FUNCTION OF SYNCHROTRON RADIATION IN RANDOM MAGNETIC FIELDS

For the case of chaotic magnetic fields one should average out the standard formula for energy distribution of synchrotron radiation

$$\frac{dN_\gamma}{dE_\gamma dt} = \frac{\sqrt{3}}{2\pi} \frac{e^3 B}{m_e c^2 \hbar E_\gamma} F\left(\frac{E_\gamma}{E_c}\right), \quad (\text{D1})$$

where

$$F(x) = x \int_x^\infty K_{5/3}(\tau) d\tau, \quad E_c = \frac{3e\hbar B \gamma^2}{2m_e c}, \quad (\text{D2})$$

over directions of magnetic field. After taking the perpendicular to velocity component of magnetic field  $B_\perp = B \sin\theta$ , where  $\theta$  is angle between  $\mathbf{B}$  and  $\mathbf{v}$  we come to the following double integral:

$$G(x) = \int \sin\theta F\left(\frac{x}{\sin\theta}\right) \frac{d\Omega}{4\pi} = \frac{1}{2} \int_0^\pi F\left(\frac{x}{\sin\theta}\right) \sin^2\theta d\theta. \quad (\text{D3})$$

After changing the order of the integration it can be written as a single integral

$$G(x) = x \int_x^\infty K_{5/3}(\xi) \sqrt{1 - \frac{x^2}{\xi^2}} d\xi, \quad (\text{D4})$$

that can be expressed in terms of modified Bessel functions:

$$G(x) = \frac{x}{20} [(8 + 3x^2)(\kappa_{1/3})^2 + x\kappa_{2/3}(2\kappa_{1/3} - 3x\kappa_{2/3})], \quad (\text{D5})$$

where  $\kappa_{1/3} = K_{1/3}(x/2)$ ,  $\kappa_{2/3} = K_{2/3}(x/2)$ . Note that while the function  $F(x)$  has a maximum at  $x = 0.2858$  ( $\max F(x) = 0.9180$ ), the maximum of the function  $G(x)$  is shifted towards smaller values:  $x = 0.2292$  ( $\max G(x) = 0.7126$ ). An alternative presentation for  $G(x)$  in terms of Whittaker's function has been derived in Ref. [27]. The functions  $F(x)$  and  $G(x)$ , as well as the ratio  $G(x)/F(x)$  are shown in Fig. 13.

Although the function  $G(x)$  in Eq. (D5) is presented in a quite compact and elegant form, for practical purposes it is convenient to have approximation which does not contain special functions. Here we propose such approximations for  $F(x)$  and  $G(x)$  which provide an accuracy better than 0.2% over the entire range of variable  $x$ :

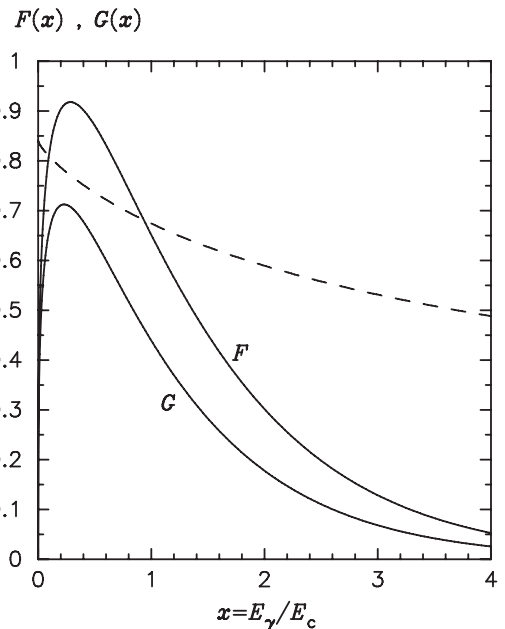


FIG. 13. The emissivity functions for synchrotron radiation  $F(x)$  and  $G(x)$ . The dashed line shows the ratio  $G(x)/F(x)$ .

$$\tilde{F}(x) \approx 2.15x^{1/3}(1 + 3.06x)^{1/6} \times \frac{1 + 0.884x^{2/3} + 0.471x^{4/3}}{1 + 1.64x^{2/3} + 0.974x^{4/3}} e^{-x}, \quad (\text{D6})$$

$$\tilde{G}(x) \approx \frac{1.808x^{1/3}}{\sqrt{1 + 3.4x^{2/3}}} \frac{1 + 2.21x^{2/3} + 0.347x^{4/3}}{1 + 1.353x^{2/3} + 0.217x^{4/3}} e^{-x}. \quad (\text{D7})$$

- 
- [1] T. Stanev, *Astrophys. J.* **479**, 290 (1997).  
 [2] J. W. Cronin, *Nucl. Phys. B, Proc. Suppl.* **138**, 465 (2005).  
 [3] F. A. Aharonian, A. A. Belyanin, E. V. Derishev, V. V. Kocharovskiy, and V. V. Kocharovskiy, *Phys. Rev. D* **66**, 023005 (2002).  
 [4] M. Vietri, *Astrophys. J.* **453**, 883 (1995); E. Waxman, *Phys. Rev. Lett.* **75**, 386 (1995); M. Milgrom and V. Usov, *Astrophys. J.* **449**, L37 (1995).  
 [5] K. Dolag, D. Grasso, V. Springel, and I. Tkachev, *J. Cosmol. Astropart. Phys.* **01** (2005) 009.  
 [6] G. Sigl, F. Miniati, and T. A. Enßlin, *Phys. Rev. D* **70**, 043007 (2004).  
 [7] N. Globus, D. Allard, and E. Parizot, *Astron. Astrophys.* **479**, 97 (2008).  
 [8] K. Kotera and M. Lemoine, *Phys. Rev. D* **77**, 023005 (2008).  
 [9] F. A. Aharonian, *Mon. Not. R. Astron. Soc.* **332**, 215 (2002).  
 [10] S. Gabici and F. A. Aharonian, *Phys. Rev. Lett.* **95**, 251102 (2005).  
 [11] F. A. Aharonian, P. S. Coppi, and H. J. Völk, *Astrophys. J.* **423**, L5 (1994).  
 [12] V. S. Berezhinsky and A. Yu. Smirnov, *Astrophys. Space Sci.* **32**, 461 (1975); P. S. Coppi and F. A. Aharonian, *Astrophys. J.* **487**, L9 (1997); O. E. Kalashev, D. V. Semikoz, and G. Sigl, *Phys. Rev. D* **79**, 063005 (2009).  
 [13] S. Gabici and F. A. Aharonian, *Astrophys. Space Sci.* **309**, 465 (2007).  
 [14] A. Yelyiv, A. Neronov, and D. V. Semikoz, *Phys. Rev. D* **80**, 023010 (2009).  
 [15] L. Eyges, *Phys. Rev.* **74**, 1534 (1948).  
 [16] V. S. Remizovich, D. B. Rogozkin, and M. I. Ryazanov, *Charged Particles Path-Length Fluctuation* (Energoatomizdat, Moscow, 1988).  
 [17] S. R. Kelner and F. A. Aharonian, *Phys. Rev. D* **78**, 034013 (2008).  
 [18] E. Waxman and J. Miralda-Escude, *Astrophys. J.* **472**, L89 (1996).  
 [19] P. G. Tinyakov and I. I. Tkachev, *Astropart. Phys.* **24**, 32 (2005).  
 [20] V. Berezhinsky, A. Gazizov, and S. Grigorieva, *Phys. Rev. D* **74**, 043005 (2006).  
 [21] A. Mücke, R. Engel, J. P. Rachen, R. J. Protheroe, and T. Stanev, *Comput. Phys. Commun.* **124**, 290 (2000).  
 [22] F. A. Aharonian and J. W. Cronin, *Phys. Rev. D* **50**, 1892 (1994).  
 [23] F. A. Aharonian, A. N. Timokhin, and A. V. Plyasheshnikov, *Astron. Astrophys.* **384**, 834 (2002).  
 [24] R. J. Protheroe and P. L. Biermann, *Astropart. Phys.* **6**, 45 (1996).  
 [25] C. Alcock and H. Hatchett, *Astrophys. J.* **222**, 456 (1978).  
 [26] J. Einasto, *New Astron. Rev.* **45**, 355 (2001).  
 [27] A. Crusius and R. Schlickeiser, *Astron. Astrophys.* **164**, L16 (1986).